

Precursor Transformation during Molecular Oxidation Catalysis with Organometallic Iridium Complexes

Ulrich Hintermair,^{§,||} Stafford W. Sheehan,[§] Alexander R. Parent,^{§,⊥} Daniel H. Ess,^{*,†} David T. Richens,^{*,‡} Patrick H. Vaccaro,^{*,§} Gary W. Brudvig,^{*,§} and Robert H. Crabtree^{*,§}

[†]Department of Chemistry & Biochemistry, Brigham Young University, Provo, Utah 84602, United States

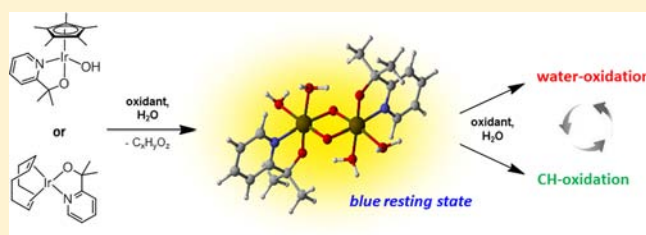
[‡]Department of Chemistry & Biochemistry, New Mexico State University, Las Cruces, New Mexico 88003, United States

[§]Department of Chemistry, Yale University, New Haven, Connecticut 06520, United States

Supporting Information

ABSTRACT: We present evidence for Cp* being a sacrificial placeholder ligand in the [Cp*Ir^{III}(chelate)X] series of homogeneous oxidation catalysts. UV–vis and ¹H NMR profiles as well as MALDI-MS data show a rapid and irreversible loss of the Cp* ligand under reaction conditions, which likely proceeds through an intramolecular inner-sphere oxidation pathway reminiscent of the reductive in situ elimination of diolefin placeholder ligands in hydrogenation catalysis by [(diene)M^I(L,L')]⁺ (M = Rh and Ir) precursors.

When oxidatively stable chelate ligands are bound to the iridium in addition to the Cp*, the oxidized precursors yield homogeneous solutions with a characteristic blue color that remain active in both water- and CH-oxidation catalysis without further induction period. Electrophoresis suggests the presence of well-defined Ir-cations, and TEM-EDX, XPS, ¹⁷O NMR, and resonance-Raman spectroscopy data are most consistent with the molecular identity of the blue species to be a bis-μ-oxo di-iridium(IV) coordination compound with two waters and one chelate ligand bound to each metal. DFT calculations give insight into the electronic structure of this catalyst resting state, and time-dependent simulations agree with the assignments of the experimental spectroscopic data. [(cod)Ir^I(chelate)] precursors bearing the same chelate ligands are shown to be equally effective precatalysts for both water- and CH-oxidations using NaIO₄ as chemical oxidant.



INTRODUCTION

Since our initial report in 2009,¹ organometallic Cp*Ir^{III} complexes (Cp* = pentamethyl-cyclopentadienyl, C₅Me₅⁻) have continued to demonstrate promising potential in water-^{2–9} and CH-oxidation^{10–12} catalysis (Figure 1). The development of efficient catalysts for these both kinetically and thermodynamically challenging reactions is of intense current interest. The water-oxidation half-reaction represents the energetic bottleneck for its use as sustainable source of electrons and protons as clean and renewable fuel in solar energy conversion schemes,^{13–20} and water-oxidation catalysts are crucial for maximizing overall efficiency.²¹ Selective CH-oxidations are key to the upgrading of unreactive feedstocks^{22–25} and the development of new synthetic methodologies,^{26–28} and only through the use of suitable catalysts may selectivity be steered in a desired way and avoid over-oxidation.²⁹ Cp*Ir^{III} precatalysts have afforded high rates and turnover numbers in water-oxidation (WO) catalysis,^{2,9} and catalytic CH-oxygenations (CHO) proceed with retention of configuration at carbon¹⁰ and good functional group tolerance.¹²

Rational catalyst development enabling efficient application is contingent upon a thorough understanding of their mode of action. Well-defined molecular systems promise to be more

amenable to mechanistic studies and systematic fine-tuning than bulk metal–oxide catalysts,^{30,31} but due to the harsh conditions required to drive these demanding oxidations, little experimental insight into the catalytic cycle has been obtained so far for the iridium systems. Only if we know which ligands are retained throughout the cycle can we design better catalysts, but while the high reaction rates of the Cp*Ir^{III} precursors are particularly promising they ironically add to the difficulty of investigating their mechanism. We have previously suggested a plausible catalytic cycle supported by DFT calculations² and studied some model intermediates,^{32,33} but now we present results of detailed experimental investigations on precatalyst transformation under reaction conditions that led to the characterization of a catalytically relevant intermediate for the first time.

We³⁴ and others⁶ have previously observed that a common feature of virtually all active Ir-WOCs is that under turnover conditions they evolve to a deeply blue colored solution with a characteristic absorption around 600 nm in the UV–vis spectrum. Although this has often been equated with the presence of IrO_x nanoparticles (NPs) in solution,^{6,35,36} we have

Received: May 15, 2013

Published: July 3, 2013

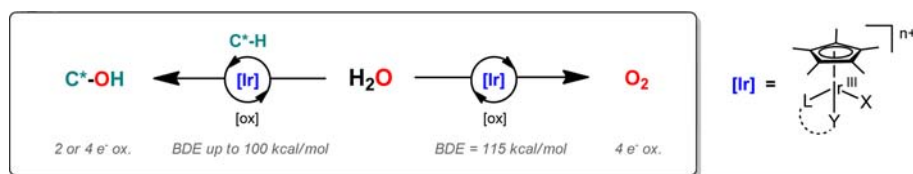


Figure 1. Oxidations catalyzed by $\text{Cp}^*\text{Ir}^{\text{III}}$ precursors ($[\text{ox}]$ = oxidant, BDE refers to substrates activated, $\text{Y} = \text{L}$ or X).

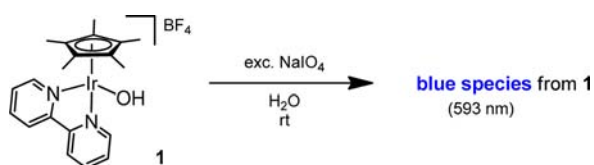
shown that when $\text{Cp}^*\text{Ir}^{\text{III}}$ precursors bearing oxidation-resistant chelate ligands (i.e., 2,2'-bipyridine [bipy] or 2-(2'-pyridyl)-2-propanolate [pyalc]) are employed, these reactive blue solutions are truly homogeneous. We have excluded the presence of nanoparticles when using chemical oxidants by time-resolved dynamic light scattering (DLS),³⁴ shown that no heterogeneous material deposits on the anode when using an electrochemical potential by electrochemical quartz-crystal nanobalance (EQCN) experiments,³⁷ and demonstrated that they display molecular kinetics distinct from those of classical IrO_2 NPs.² On the basis of the observed ligand effects on the resistance toward NP formation and on the λ_{max} of the resulting particle-free blue solutions, we proposed retention of the chelate ligand in a molecular blue species.³⁴ The fate of the Cp^* ligand, the molecular identity of the blue species, and its kinetic relevance to catalysis, however, are important questions that remained to be answered. Both nucleophilic attack of the benzylic $\text{CH}'\text{s}$ ^{38–41} as well as electrophilic attack on the quaternary carbons^{42,43} of Cp^* are known for half-sandwich complexes of iridium, and several studies have reported Cp^* modification under oxidative conditions,^{6,41,42} without a clear interpretation as to what this means for the catalysis, however. A recent study on functionalized Cp^*Ir WOCs embedded in a porous solid, which appeared while this work was in progress, reported some evidence for Cp^* -free iridium species as precatalyst derivatives.⁴⁴ Here, we present our results of detailed kinetic and spectroscopic investigations on solution-phase oxidation catalysis using homogeneous $\text{Cp}^*\text{Ir}^{\text{III}}$ precursors with NaIO_4 as mild chemical oxidant^{45,46} that answer some of the above-mentioned questions, and draw a clearer picture of how these promising systems function on the molecular level.

RESULTS AND DISCUSSION

We started studying the oxidative transformation on the relatively slowly reacting precatalyst $[\text{Cp}^*\text{Ir}(\text{bipy})\text{OH}]\text{BF}_4$ (**1**). Monitoring the reaction of **1** with excess NaIO_4 in H_2O (Scheme 1) by UV–vis spectroscopy showed a smooth evolution of the characteristic $\lambda_{\text{max}} \sim 590$ nm over the course of several minutes (Figure 2, left), well suited for kinetic studies.

Variation of iridium concentration showed the rate of the reaction to be independent of $[\text{Ir}]$ over more than 1 order of magnitude (Figure 2, right), whereas variation of NaIO_4

Scheme 1. Oxidation of Yellow $[\text{Cp}^*\text{Ir}(\text{bipy})\text{OH}]\text{BF}_4$ to a Blue Species



concentration showed a first-order rate dependence on oxidant (Figure 3). Thus, the rate-determining step of the formation of the blue species appears to be the initial oxidation of the Cp^* precursor, proceeding with an apparent first-order rate constant $k_{\text{obs}} = 0.08 \pm 0.01 \text{ s}^{-1}$ that corresponds to a half-life time of about 9 s for **1** under these conditions. Furthermore, every metal center appears to contribute equally to the electronic transition at ~ 590 nm because identical final molar absorptivities of $\epsilon_{590} = 1850 \pm 50 \text{ M}^{-1} \text{ cm}^{-1}$ were found over a wide range of iridium concentrations (Figure 2, right).

Monitoring the reaction of **1** with excess NaIO_4 in H_2O by ^1H NMR analysis of sampled aliquots quenched with NaHSO_3 showed a progressive disappearance of the Cp^* peak over time with build-up of acetic acid to a final level of ~ 1.8 equiv per $[\text{Ir}]$ (Figure 4, left). No signals from partially oxidized **1** or other organic fragments were detected by ^1H and ^{13}C NMR, but some split and broadened peaks of the bipy ligand remained visible in the aromatic region (Figures S1 and S2). Importantly, monitoring the reaction by UV–vis spectroscopy under the same conditions showed Cp^* loss to be concomitant with build-up of the absorption at 590 nm (Figure 4, right), suggesting the blue species to be an oxidized form of **1** lacking the Cp^* ligand.

To test how the Cp^* ligand is oxidatively removed from the Ir^{III} precursor, the coordinatively saturated sandwich complex $[\text{Cp}^*\text{Ir}(\text{tacn})\text{SO}_4]$ (**2**, $\text{tacn} = 1,3,5$ -triazacyclononane) was prepared and treated with excess NaIO_4 in H_2O (Scheme 2). In this case, the ^1H NMR and UV–vis spectra of the complex remained entirely unchanged, and no O_2 evolution was detectable by Clark-type electrode (Figures S5–S7). The complete inertness of **2** toward oxidation demonstrates that neither direct oxidant attack on the coordinated Cp^* ligand nor outer-sphere electron transfer from the Ir^{III} to the oxidant seem to take place, and oxidative transformation of $\text{Cp}^*\text{Ir}^{\text{III}}$ complexes thus occurs within the coordination sphere of the metal, requiring at least one open site to proceed. While $[\text{Cp}^*\text{Ir}(\text{bipy})\text{X}]^+$ complexes with various hydrolyzable X ligands readily react with aqueous periodate, no reaction occurred between $[\text{Cp}^*\text{Ir}(\text{bipy})\text{Cl}]\text{BF}_4$ and $[\text{NBu}_4][\text{IO}_4]$ in dry CH_2Cl_2 (Scheme 3 and Figures S3 and S4). Thus, in addition to an open site, water is also needed for oxidative activation of the $\text{Cp}^*\text{Ir}^{\text{III}}$ complex with NaIO_4 , either by providing an $\text{Ir}-\text{OH}_{(2)}$ moiety on the precursor, through hydration of the oxidant, or both. When a 1:1 mixture of **1** and **2** was treated with excess NaIO_4 in water, the Cp^* peak of **1** quickly disappeared from the ^1H NMR spectrum as in the absence of **2**, but the Cp^* peak of **2** then also started to decrease over time with more acetic acid being formed (Figure S8). This mutual attack on the otherwise inert **2** by oxidized **1** reflects the CH-oxidation ability of these catalysts, and shows that bimolecular pathways may also play a role in the initial precursor oxidation. This observation is important with regards to traces of easily oxidizable iridium impurities potentially carried through to catalytic mixtures from the synthesis.⁴⁷

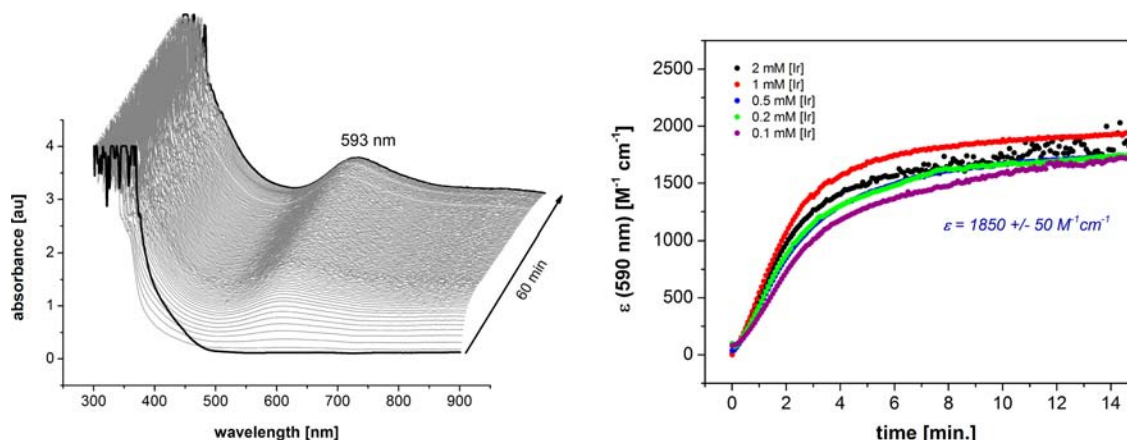


Figure 2. Full scan UV–vis time-course of the reaction shown in Scheme 1 at 1 mM [Ir] + 100 mM NaIO₄ (left), and kinetics of the 590 nm absorption band at 100 mM NaIO₄ (right).

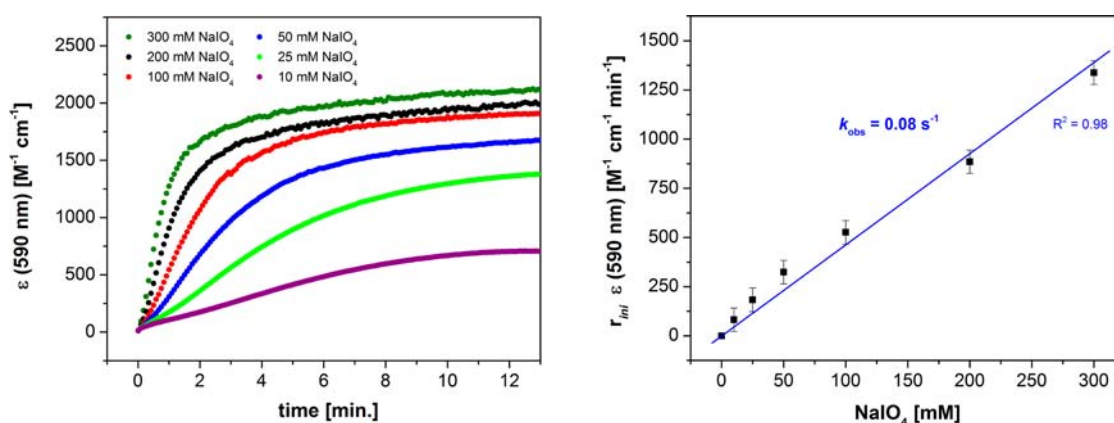


Figure 3. UV–vis kinetics of the reaction shown in Scheme 1 at 1 mM [Ir] monitored at 590 nm.

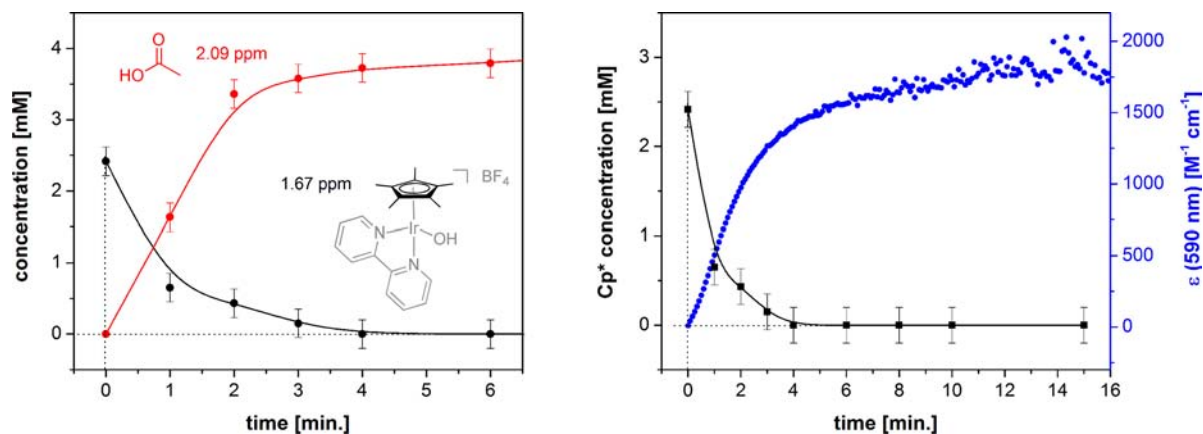
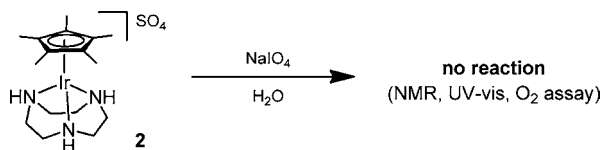


Figure 4. ¹H NMR time-course of the reaction of **1** at 2 mM with 100 mM NaIO₄ in H₂O as measured from sampled aliquots quenched with NaHSO₃ + sodium *d*₄-trimethylsilylpropionate (20 mM) in D₂O (left), and comparison with UV–vis kinetics of the same reaction monitored at 590 nm (right).

Scheme 2. Inertness of [Cp*Ir(tacn)]SO₄ toward Oxidation with Aqueous NaIO₄



Depending on the initial oxidant/[Ir] ratio, the blue species of oxidized **1** decayed after longer times in solution (Figure 5, left). Such behavior has previously been observed for other Cp*Ir^{III} precursors when oxidized with Ce^{IV}, and it was speculated that the corresponding blue species were highly activated intermediates whose decay directly yields O₂.⁴⁸ Monitoring the 590 nm band intensity during O₂ evolution with **1** and NaIO₄ clearly showed, however, that the blue species built up as the rate of O₂ production decreased, and

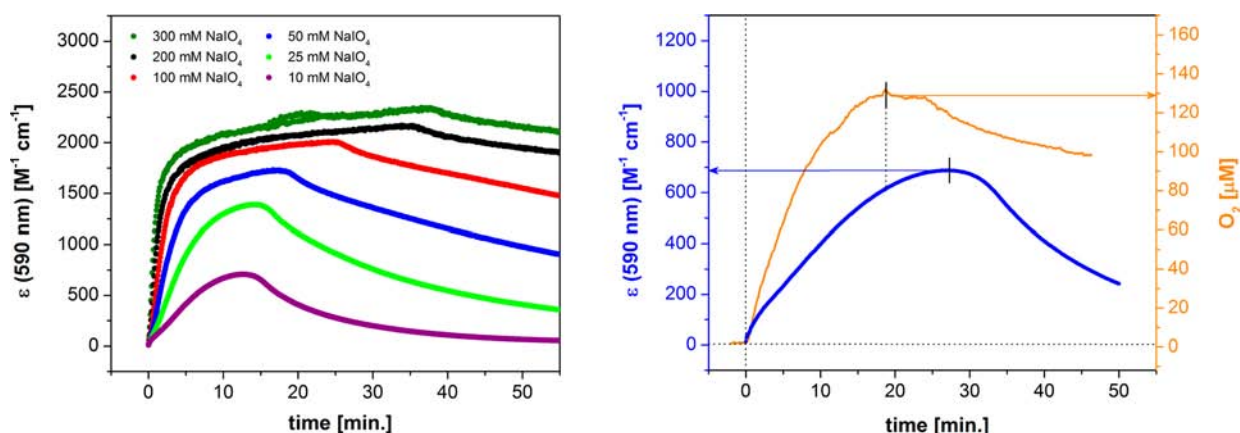
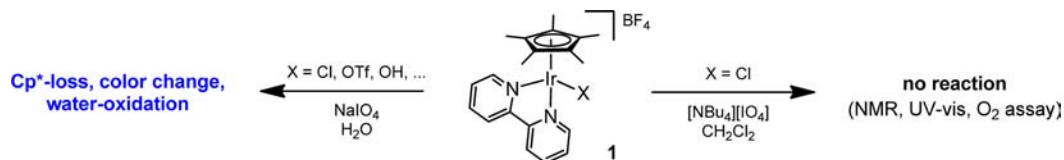
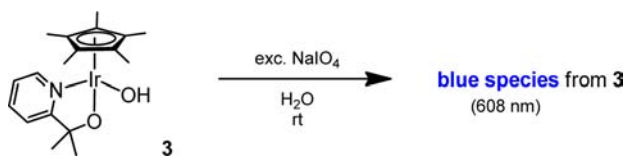
Scheme 3. Reactivity of $[\text{Cp}^*\text{Ir}(\text{bipy})\text{X}]\text{BF}_4$ Complexes with Periodate

Figure 5. UV-vis kinetics of the reaction shown in Scheme 1 at 1 mM [Ir] monitored at 590 nm (left), and 590 nm intensity versus O_2 evolution of the same reaction at 0.2 mM [Ir] + 10 mM NaIO_4 (right).

then decayed only after O_2 evolution had ceased (Figure 5, right). This behavior is a classical kinetic trace of a metastable intermediate that may be either a catalyst resting or a deactivation state.⁴⁹ Because of the limited lifetime of the blue species from oxidized **1** attention was turned to other precursors for more detailed studies.

$\text{Cp}^*\text{Ir}^{\text{III}}$ complexes bearing the more strongly donating LX-type pycal ligand (**3**, Scheme 4) yielded more rapid color

Scheme 4. Oxidation of Orange $[\text{Cp}^*\text{Ir}(\text{pyalc})\text{OH}]$ to a Blue Species

changes with an apparent first-order rate constant of $\sim 0.4 \pm 0.1 \text{ s}^{-1}$ when oxidized with NaIO_4 , about 5 times faster than the bipy-based precursor. The corresponding blue species with a $\lambda_{\text{max}} \sim 608 \text{ nm}$ was found to persist for days even after complete exhaustion of oxidation potential in solution. Oxidative Cp^* loss was also quicker for **3** than for **1**, again liberating ~ 1.8 equiv of $\text{HOAc}/[\text{Ir}]$ without any other detectable organic species in solution (Figure 6). Small and broadened ligand peaks remained visible in the aromatic region of the NMR spectrum as in the case of **1** (Figure S9).

To test whether the stable blue species from **3** may resume its catalytic activity once formed, O_2 evolution was monitored during multiple additions of aqueous NaIO_4 to a dilute solution of **3** (Figure 7). Under the conditions applied, an initial induction period of about 2 min before O_2 evolution set in was observed, which shortens to a minimum of $\sim 10 \text{ s}$ at higher concentrations (see below). Thereafter, production of $\sim 3 \text{ TON}$

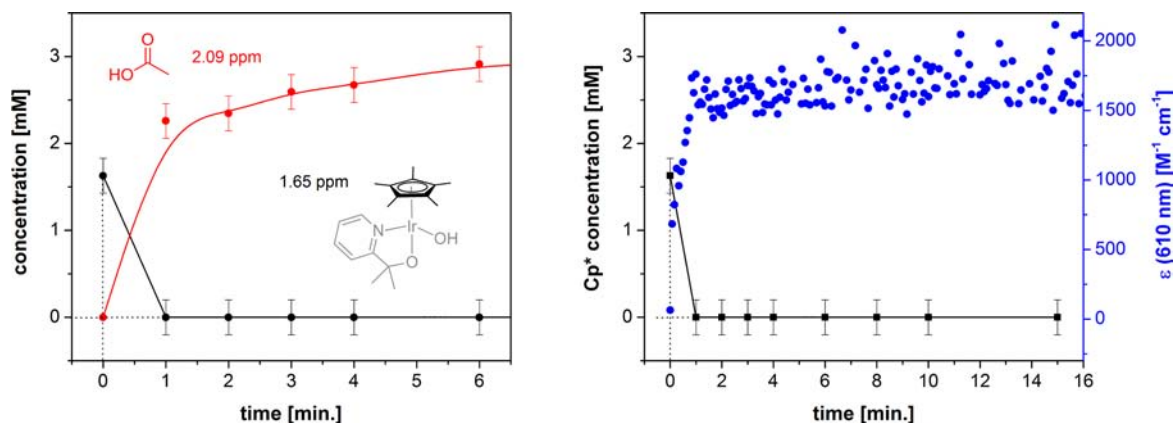


Figure 6. ^1H NMR time-course of the reaction of **3** at 2 mM with 100 mM NaIO_4 in H_2O as measured from sampled aliquots quenched with NaHSO_3 + sodium d_4 -trimethylsilylpropionate (20 mM) in D_2O (left), and comparison with UV-vis kinetics of the same reaction monitored at 610 nm (right).

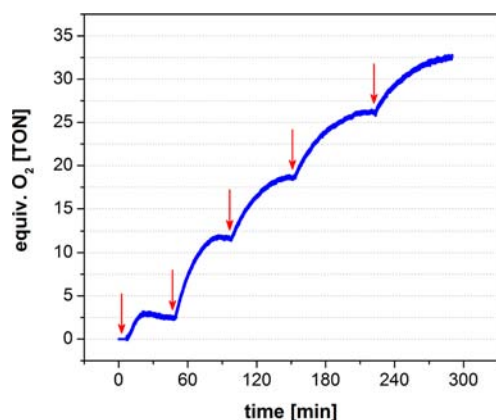


Figure 7. O₂ production of **3** at 4 μM during multiple additions of 34 equiv of NaIO₄ in H₂O (arrows) as measured by Clark-type electrode in the liquid phase (rates decrease due to successive dilution).

(turnover numbers) of O₂ quickly occurred. Repeated additions of the same amount of NaIO₄ to the same solution then caused immediate O₂ production with increased efficiencies of average 7.5 TON to O₂ over at least four cycles.⁵⁰ Such sustained oxidation activity has been described earlier for various Ir precursors oxidized with Ce^{IV}, but was interpreted as oxidative loss of all ligands and decomposition to IrO_x NPs as the true active catalyst.⁶ In this case, we can exclude this possibility based on the observed ligand effects and our dynamic light scattering results, which showed the system **3** + NaIO₄ to be genuinely homogeneous.³⁴

Similarly, the catalytic CH-oxidation activity of **3** could also be sustained, and cumulating turnover numbers were obtained upon multiple additions of ethylbenzene-sulfonate (EBS) and NaIO₄ to an aqueous solution of **3** (Scheme 5 and Table 1).

Scheme 5. Methylene Oxidation of Ethylbenzene-sulfonate (EBS) to Acetophenone-sulfonate (APS) with NaIO₄ Catalyzed by **3**

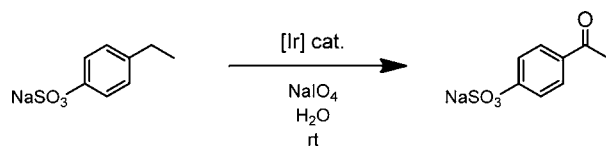


Table 1. Activity of **3 at 0.5 mM in Catalytic EBS Oxidation (Scheme 5) upon Multiple Additions of Substrate and Oxidant**

EBS (equiv)	NaIO ₄ (equiv)	reaction time (min)	TON to APS
20	200	30	13 (±2)
40	400	60	32 (±2)
60	600	90	41 (±2)
80	800	120	52 (±2)

These observations have at least two important implications. Clearly, the Cp*-free blue molecular species formed after initial oxidation is either an in-cycle catalytic intermediate or an off-cycle resting state. Furthermore, the fact that an induction period is only initially observed and that unperturbed performance occurs upon reoxidation suggests that intramolecular loss of the Cp* ligand precedes intermolecular turnover in the case of **3**, and is thus a precursor activation step rather than a decomposition pathway as previously suggested

for other Cp*Ir^{III} precatalysts in the presence of ceric ammonium nitrate (CAN).^{6,42,43} These findings agree well with a recent report on highly efficient water-oxidation catalysis by Cp*Ir^{III} precursors preactivated with NaIO₄.⁹

Many stable, high-valent Cp* metal-oxo complexes of the middle transition metals Cr,⁵¹ Mo,⁵² W,⁵³ and Re⁵⁴ are known, but these generally only oxidize activated substrates (e.g., olefin-epoxidation). To the best of our knowledge, no stable Cp*M=O complexes of the platinum group metals are known, although some Cp*Ru-μ-oxo,⁵⁵ Cp*Ru-peroxo,⁵⁶ and Cp*Os-μ-oxo⁵⁷ species have been reported. Being on the brink of the oxo-wall,⁵⁸ an octahedral d⁴ Ir^V-oxo can be expected to be highly reactive,⁵⁹ and it is thus not surprising that the Cp* ligand would be thermodynamically unstable on such a strongly oxidizing intermediate. More importantly, however, the data reported here provide evidence that it is also kinetically unstable, and thus unlikely to be part of an intermolecular oxidation cycle.

Although remarkably robust in solution, isolation of the blue species of oxidized **3** from its native aqueous solution in pure form proved difficult, and more detailed characterizations were thus performed on the solution. Electrophoresis of a solution of oxidized **3** showed a clean migration of the blue compound toward the negatively charged electrode without separation of any other colored component, suggesting the presence of a single, well-defined iridium-cation (Figure 8).

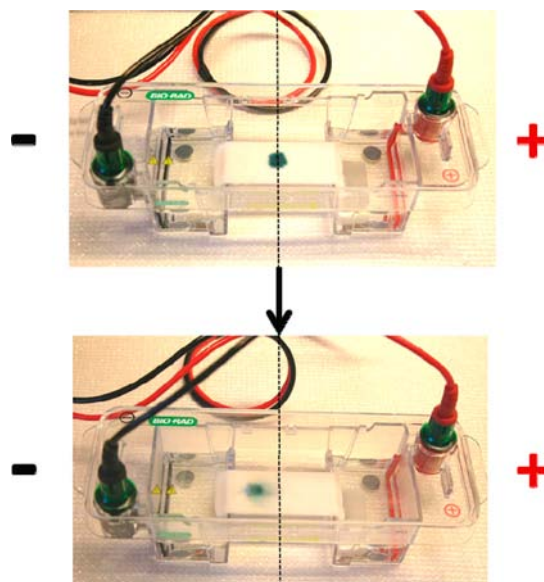


Figure 8. Planar electrophoresis of 1 mL of a solution of **3** (10 mM) oxidized with NaIO₄ (200 mM) on a glass-microfiber support in 100 mM aqueous NaIO₃ electrolyte with 100 mA at 120 V for 10 min.

MALDI-TOF-MS(+) analysis (matrix-assisted laser desorption/ionization time-of-flight mass spectrometry) of partially oxidized **3** from a reducing matrix showed several [Cp*Ir-(pyalc)]⁺ + [O] species indicating successive oxygenation of the precursor,⁶⁰ as well as Cp*-free dimers with iridium in the (III) oxidation state (Figure 9 and Figures S10–S14). Simulation of these peaks agreed with their assignment as [Ir₂(pyalc)₂(O)₂H]⁺ at a high accuracy of 44 ppm. Such dimers would be fully consistent with all previous observations on oxidative Cp* loss under preservation of the chelate ligand, and similar bis-μ-hydroxy aqua-dimers of iridium are known to be

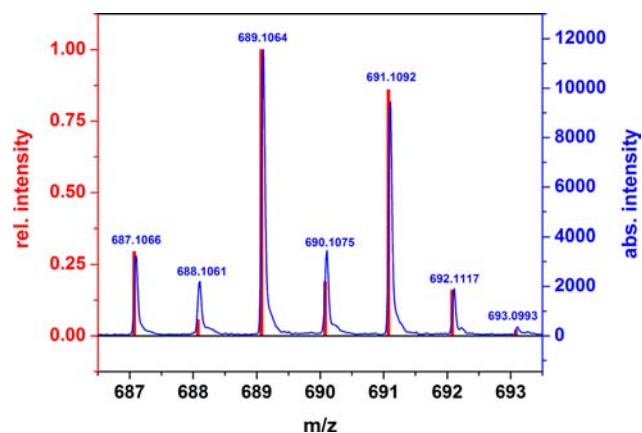


Figure 9. Section of the experimental MALDI-TOF-MS(+) spectrum of a sample of **3** oxidized with NaIO_4 as obtained from α -cyano-4-hydroxycinnamic acid matrix (blue curve and values), and simulation for $[\text{Ir}_2(\text{pyalc})_2(\text{O})_2\text{H}]^+ = \text{C}_{16}\text{H}_{21}\text{Ir}_2\text{N}_2\text{O}_4^+$ (red bars).

blue with a $\lambda_{\text{max}} \sim 590$ nm in the (IV) oxidation state.⁶¹ No iodine-containing adducts were detected by MS and no peaks above 1200 m/z were observed (Figure S11), excluding the presence of higher nuclearity clusters or nanoparticles^{62–64} consistent with our previous light scattering results.³⁴

TEM-EDX analysis (transmission electron microscopy-energy-dispersive X-ray spectroscopy) showed the presence of both carbon and nitrogen in a sample of fully oxidized **3** dried to a powder in high vacuum (Figure 10). Although carbon was

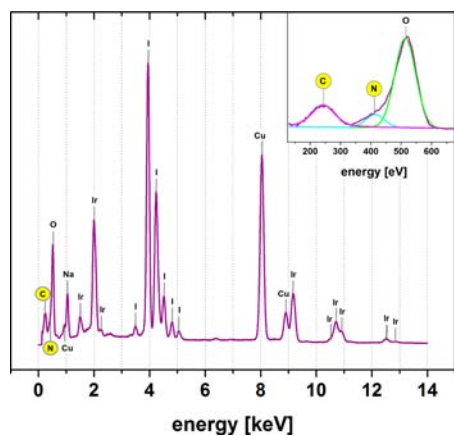


Figure 10. EDX spectrum (200 kV) of a sample of vacuum-dried blue species from **3** (including the reduced form of the oxidant NaIO_4) showing the presence of C, N, O, Na, I, and Ir (Cu signals arise from the TEM grid) with deconvoluted peaks of the C/N/O region shown in the inset.

not securely quantifiable due to background from adventitious carbon, a clear 1:1 ratio of N to Ir was found as further indication for the retention of the chelate ligand in the blue species consistent with the MS analysis. When exposed to the focused electron beam for longer times (>30 s), the material progressively decomposed to form ~ 7 Å domains of rutile IrO_2 (Figures S15–S17). This observation shows how easily electron microscopy can induce sample changes to suggest catalyst decomposition into particles, and is therefore not an entirely reliable method for distinguishing homogeneous from heterogeneous catalysts on its own.

XPS analysis (X-ray photoelectron spectroscopy) of the same sample on ultrapure gold also showed N-1s and C-1s signals, the latter comprising sp^2 carbon (284.8 eV), ortho-nitrogen carbon (286.7 eV), and sp^3 carbon neighboring oxygen (287.9 eV) (Figure 11, left).^{65,66} Consistent with the quantification by EDX, an approximate 1:1 ratio of N to Ir was found again (Figure S18). The Ir-4f doublet observed at 62.4 and 65.3 eV, although overlapping with the Na-2s signal from the oxidant at 63.9 eV (Figure 11, right), is fully consistent with iridium being exclusively in the (IV) oxidation state when compared to literature values.⁶⁷ The solid material retained its blue color under brief X-ray irradiation, suggesting retention of its native oxidation state during the course of the analysis. Lin had previously observed reduction of an oxidized bipy-based $\text{Cp}^*\text{Ir-WOC}$ under XPS conditions to only see Ir^{III} at 60.7 and 63.8 eV,⁴⁴ and the higher stability of the blue species derived from the pycal-ligated precursor **3** likely contributes to this difference. Although some oxo-centered acetate trimers⁶⁸ and nitrido-centered sulfate trimers⁶⁹ of iridium are known to be remarkably stable in (III)–(IV) mixed-valent states, the presence of stoichiometric amounts of Ir^{III} in the blue species of **3** can be ruled out by the lack of any distinguishable peak in the 60–61 eV region in the XPS analysis.

An open-shell Ir^{IV} would account for the ill-defined NMR signals of the chelate ligand in solutions of the blue species. EPR (electron paramagnetic resonance) spectroscopy at 7 K, however, did not show any signal either, suggesting an even-numbered polynuclear species with coupled d^5 metal centers to give a net zero electronic spin in the ground state.⁷⁰ At room temperature, a weak paramagnetic moment corresponding to ~ 0.6 unpaired electrons per iridium could be detected by the Evans method in solution (Figure S19). The clean migration of the blue species in the electrophoresis agrees less with dimerization equilibria of d^5 monomers, and rather suggests the presence of a well-defined polynuclear species with electronically coupled Ir^{IV} centers.

Complete departure of Cp^* from the metal with retention of the chelate ligand would leave each iridium with four open sites, which would most likely be occupied by oxo, hydroxo, or aqua ligands under oxidative conditions in water. Mononuclear metal-aqua ion chemistry is well-established even for the less oxophilic late transition metals,^{71,72} and polynuclear oxy-bridged aqua-clusters are also known.⁷³ Several μ -oxy dimers of d^6 metal centers, that is, those of Co^{III} ,^{74–76} Rh^{III} ,^{77–79} and Ir^{III} ,⁸⁰ have been reported, but only one Ir^{IV} μ -oxy-dimer⁸¹ has been characterized so far. ^{17}O NMR is the method of choice to probe the solution chemistry of such aqua-⁸² and polyoxo-ions,⁸³ but has rarely been used to investigate functional water-oxidation catalysts.^{84,85} The quadrupole-broadened resonances and the large shift range of the ^{17}O nucleus (>1000 ppm) make it virtually insensitive to paramagnetic effects in solution, providing a convenient probe for metal-oxo compounds across different oxidation states.

Complex **3** dissolved in $^{17}\text{OH}_2$ (10 mM, pH ~ 9) showed one broad ^{17}O NMR signal ($w_{1/2} = 290$ Hz) at 174 ppm originating from the $\text{Ir}^{\text{III}}\text{-OH}$ exchanging with solvent (Figure S20). The strong trans-effect of Cp^* on monodentate ligands in the otherwise extremely slow-exchanging⁸⁶ d^6 Ir^{III} aqua-complexes is well documented,⁸⁷ and in this case enhanced further by the π -basic pycal ligand.^{88,89} NaIO_4 in $^{17}\text{OH}_2$ (200 mM, pH ~ 5) gave a characteristic, broad signal from 210 to 260 ppm (centered at 236 ppm, $w_{1/2} = 2300$ Hz) due to quadrupolar

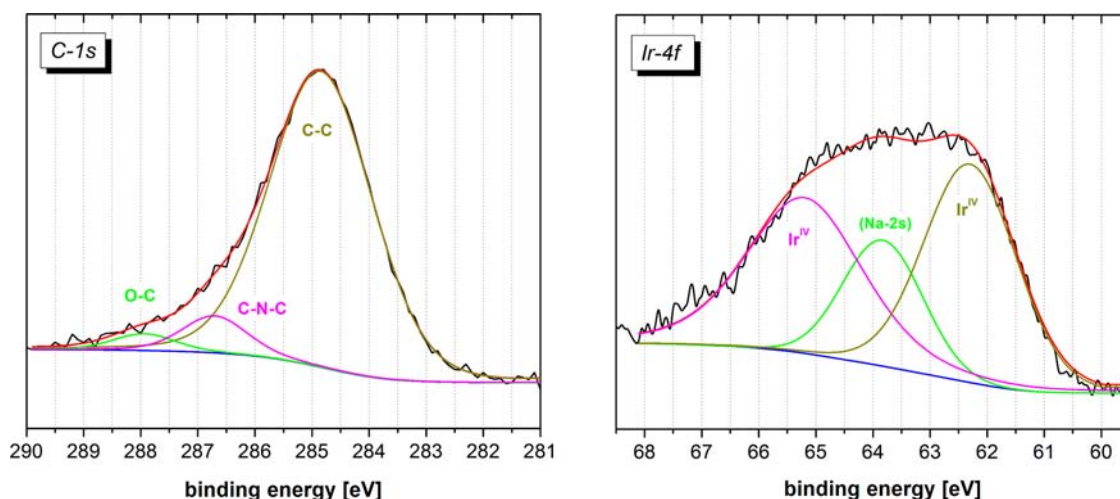


Figure 11. Carbon-1s (left) and iridium-4f sections (right) of the XPS spectrum (Al $K\alpha$ radiation) of a sample of vacuum-dried blue species from 3 (including the reduced form of the oxidant NaIO_4).

coupling of the ^{17}O with ^{127}I nuclei⁹⁰ overlaid with various hydration equilibria (Figure S21).⁹¹

Stable blue solutions of 3 oxidized with periodate in $^{17}\text{OH}_2$ showed none of the precursor or periodate peaks, but three new signals instead (Figure 12). The dominant peak at 207

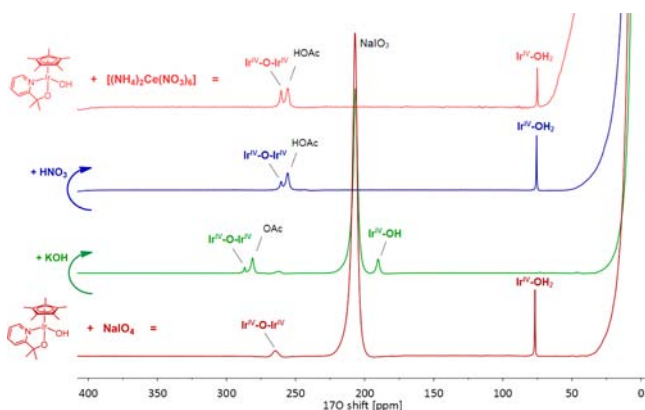


Figure 12. ^{17}O NMR spectra of 3 (10 mM) oxidized with NaIO_4 (200 mM) in 10% $^{17}\text{OH}_2$ as prepared (pH \sim 5, bottom trace), basified with KOH to pH \sim 12 (lower middle trace), and reacidified with HNO_3 to pH \sim 1 (upper middle trace) as well as 3 oxidized with CAN instead of NaIO_4 under otherwise identical conditions (top trace).

ppm ($w_{1/2} = 400$ Hz) was identified as NaIO_3 ⁹² by comparison with an authentic sample, providing spectroscopic evidence for periodate acting as a net 2-electron acceptor when driving oxidation catalysis.⁴⁶ The sharp peak at 77 ppm ($w_{1/2} = 35$ Hz) is consistent with an Ir^{IV} -aqua unit,⁸¹ while the broader signal at 265 ppm ($w_{1/2} = 340$ Hz) lies in the shift region characteristic for μ -oxo ligands.⁷³ A quantitative ^{17}O NMR spectrum showed a clean 1:2 ratio of μ -oxo to aqua peak area (Figure S22). Thus, considering the observation of dimeric species in the MS, the all- Ir^{IV} state as derived from XPS, and the $S = 0$ ground state suggested by EPR, the most plausible formulation for blue, activated 3 is $[\text{Ir}^{\text{IV}}(\text{pyalc})(\text{H}_2\text{O})_2(\mu\text{-O})]_2^{2+}$.

Polyoxy-anions, which engage in hydration equilibria such as iodate,⁹³ often bind to aqua-complexes in irreversible condensation reactions,⁹⁴ but the low nucleophilicity of the high-valent $\text{Ir}^{\text{IV}}\text{-OH}_2$ likely suppresses this reaction in this case.

To ascertain the assignment of the 77 ppm peak as coordinated water, the solution of oxidized 3 prepared in $^{17}\text{OH}_2$ was basified with KOH to pH \sim 12. No visible color changes occurred (see below), ruling out reduction of the iridium. As can be seen in Figure 12, the aqua peak shifted almost completely to 190 ppm ($w_{1/2} = 170$ Hz), assignable to the corresponding $\text{Ir}^{\text{IV}}\text{-OH}$. The μ -oxo peak also moved downfield by about 20 ppm as a result of the deprotonation, substantiating the notion that both functionalities are part of the same molecule. Reacidifying the sample with HNO_3 regenerated the initial spectrum, reforming all $\text{Ir}^{\text{IV}}\text{-OH}_2$ and shifting the μ -oxo peak back to its original position. The missing iodate peak in the acidified sample is due to the known rapid exchange with solvent water at low pH,⁹³ which is also reflected in the broadened free water peak at 0 ppm. The observation that neither the $\text{Ir}\text{-O}\text{-Ir}$ nor the $\text{Ir}\text{-OH}_2$ signals experienced measurable line shape broadening at low pH indicates surprisingly low exchange rates of both functionalities at a d^5 metal center, which probably arises from electronic coupling in the (IV)–(IV) dimer (see below). Temperature variation between 10 and 80 $^\circ\text{C}$ did not cause any changes in the ^{17}O spectrum either (Figure S23), although some dark precipitate formed above 60 $^\circ\text{C}$ at the expense of signal intensity. The fact that no noticeable line broadening occurred until thermal decomposition speaks to the remarkably high stability of the Ir^{IV} μ -oxo dimer containing the pyalc ligand.

UV-vis pH-titration of oxidized 3 with NaOH/HNO_3 determined the average $\text{p}K_{\text{A}}$ of the aqua ligands to be 5.0, consistent with high-valent $\text{Ir}^{\text{IV}}\text{-OH}_2$ species (Figure 13).⁹⁵ All spectral changes were found to be fully reversible, and a quasi-isoabsorbic point around 435 nm indicated the presence of several aqua ligands with very similar $\text{p}K_{\text{A}}$. The fact that no further spectral changes became apparent at low pH values suggests the $\text{p}K_{\text{A}}$ of the oxo bridges to be <2 , confirming the high hydrolytic stability suggested by the ^{17}O NMR results. This is in good agreement with a related bis- μ -oxo Ir^{III} aqua dimer, for whose oxo bridges a $\text{p}K_{\text{A}}$ of 1.6 has been reported.⁸¹

Upon raising the pH of the blue solution of 3 oxidized with NaIO_4 , acetate appeared in the ^{17}O NMR spectrum at 280 ppm and acetic acid persisted at 255 ppm⁹⁶ after reacidifying (as verified by spiking with authentic HOAc). The fact that (H)OAc was initially not visible in the ^{17}O NMR in solutions of

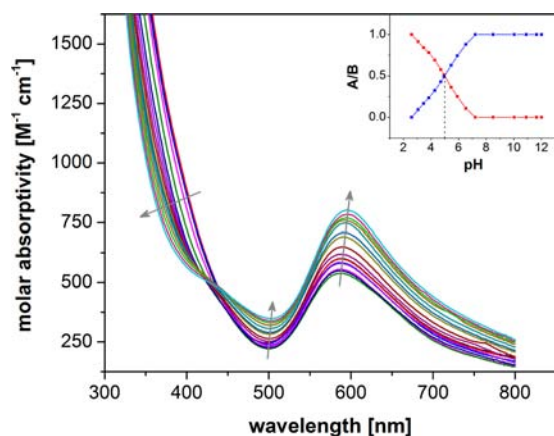


Figure 13. UV-vis spectra of **3** (0.5 mM) oxidized with NaIO_4 (135 mM) in water during pH-titration with NaOH/HNO_3 (arrows indicate changes observed upon lowering the pH). The inset shows the $\text{Ir}-\text{OH}_2$ (A, red) to $\text{Ir}-\text{OH}$ (B, blue) ratio as determined by a global fit from 300 to 800 nm.

oxidized **3** (but clearly observable by ^1H and ^{13}C NMR, see above) suggests that its formation through Cp^* oxygenation is too fast to allow for ^{17}O incorporation from the solvent. O-exchange reactions of carboxylic acids in water are known to be very slow at neutral pH but are both acid- and base-catalyzed,⁹⁷ so $(\text{H})\text{OAc}$ only becomes visible in the ^{17}O spectrum upon postsynthetic pH variation. No other oxycarbon species⁹⁸ were detected by ^{17}O NMR.

Importantly, when **3** was oxidized with CAN instead of NaIO_4 in $^{17}\text{OH}_2$, a virtually identical spectrum was obtained as after addition of HNO_3 to the sample oxidized with NaIO_4 (Figure 12, top trace). This strongly suggests that at least in the case of **3** the formation of the blue Ir^{IV} μ -oxo dimer is not influenced by the nature of the chemical oxidant.

To ascertain our spectroscopic assignments and gain deeper insight into the structure of the blue Ir^{IV} species, we modeled the dicationic $[\text{Ir}^{\text{IV}}(\text{pyalc})(\text{H}_2\text{O})_2(\mu\text{-O})]_2$ complex by density functional theory (DFT). All calculations were carried out in Gaussian 09,⁹⁹ and structures were optimized with the M06 functional¹⁰⁰ and the LANL2DZ basis set for iridium and 6-31G(d) basis set for all other atoms. Optimizations were carried out using the PCM model for water solvent.¹⁰¹

Five stable geometries of an Ir^{IV} bis- μ -oxo aqua dimer bearing the pyalc ligand were investigated (Figure 14, see the

Supporting Information for coordinates). The S_{2n} symmetric *cis*-aqua isomer **I** with both pyalc ligands *trans* to each other was found to be the most stable, fitting the intuitive expectation that the weak aqua ligands would prefer positions *trans* to the strongly donating oxo ligands. Although not fully equivalent by symmetry, the electronic environments of the two sets of aqua ligands in **I** (*trans*- μ -oxo and *trans*-alkoxide) are plausibly too similar to be distinguishable by ^{17}O NMR. Swinging one pyalc ligand around to position both pyridines *trans* to the same μ -oxo ligand as in **II** was found to be less favorable by 7 kcal/mol. Switching the coordination mode of one pyalc to have an alkoxide *trans* to a μ -oxo as in **III** was also 7 kcal/mol higher in energy relative to **I**. Putting both alkoxide moieties on the same side of the dimer as is **IV**, effectively eliminating the possibility of intramolecular aqua-alkoxide hydrogen bonding, was found to be less favorable by 12 kcal/mol, although this trend is probably overestimated by the discrete modeling and expected to be less pronounced in aqueous solution. Forcing the two pyalc ligands completely into the $\text{Ir}-\text{O}-\text{Ir}$ plane as in **V**, a combination of the detrimental effects observed in **II**–**IV**, resulted in a net destabilization of 25 kcal/mol relative to **I**.

Examination of the singlet DFT wave function of these complexes showed a restricted approximation instability, and reoptimization with unrestricted theory gave an $\langle \hat{S}^2 \rangle$ value of ~ 1.0 . Time-dependent DFT modeling of the UV-vis spectrum of complex **I** showed that for restricted M06 there is a very strong 663 nm excitation with an oscillator strength of 0.144. Weak excitations also appeared between 335 and 434 nm. The use of unrestricted M06 theory resulted in the UV-vis spectrum of complex **I** showing two strong excitations at 653 and 607 nm with oscillator strengths of 0.073 and 0.037 (Figure 15). These major transitions result mainly from excitation of Ir^{IV} -centered electrons into vacant $\text{Ir}=\text{O}$ $d_{\pi}-p_{\pi}^*$ orbitals. Such strong and broad absorptions in the visible 400–700 nm range are often seen with high-valent metal-oxo compounds; the related oxo-bridged d^5 dimer $[(\text{bipy})_2(\text{H}_2\text{O})\text{Ru}^{\text{III}}(\mu\text{-O})\text{-Ru}^{\text{III}}(\text{H}_2\text{O})(\text{bipy})_2]^{4+}$, for instance, is known to have a λ_{max} around 640 nm.¹⁰² Modeling of complex **I** with both iridiums in the (III) oxidation state as fully closed-shell d^6 dimer showed no major electronic excitations above 450 nm, consistent with the experimental observation that the reduced form lacks the characteristic UV-vis features above 450 nm of the (IV–IV) state (Figure S24).

We also modeled the UV-vis spectra of the corresponding doublet Ir^{IV} monomers. The monocationic $[\text{Ir}^{\text{IV}}(\text{pyalc})-$

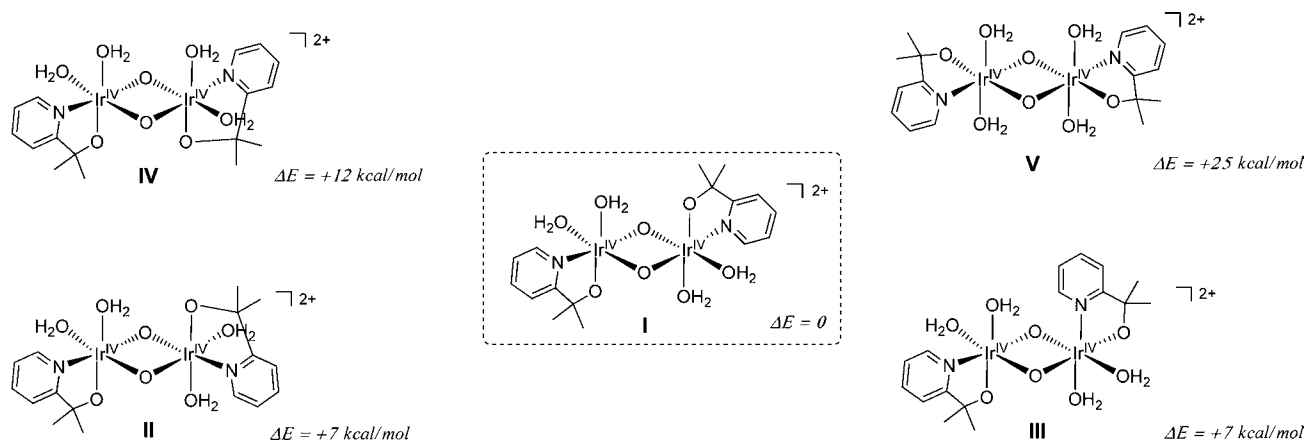


Figure 14. M06-optimized coordination isomers of $[\text{Ir}^{\text{IV}}(\text{pyalc})(\text{H}_2\text{O})_2(\mu\text{-O})]_2^{+2}$.

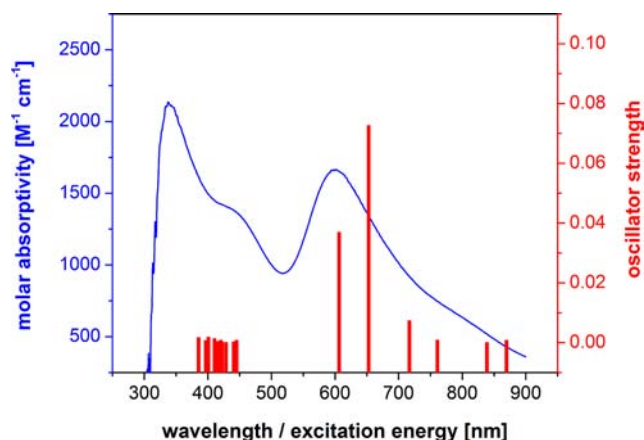


Figure 15. Experimental UV-vis spectrum of oxidized **3** (blue curve) and electronic transitions of **I** as modeled by TD-DFT (red bars). Note that single oscillator strengths are not quantitatively comparable to experimentally observed intensities.

(H_2O)₂(OH)₂] complex, potentially formed by hydrolytic cleavage of the bis- μ -oxo dimer, showed the major contribution to its UV-vis spectrum to be an excitation at 488 nm (Figure S25). Modeling of the tautomeric $[\text{Ir}^{\text{IV}}(\text{pyalc})(\text{H}_2\text{O})_3(\text{O})]^+$ revealed that in the ground state this complex prefers the oxo ligand *trans* to an aqua ligand, and forcing the oxo *trans* to the nitrogen of the pyalc ligand would be 12 kcal/mol higher in energy. The major contributions to the UV-vis spectrum of the low-energy isomer of $[\text{Ir}^{\text{IV}}(\text{pyalc})(\text{H}_2\text{O})_3(\text{O})]^+$ were found to be excitations at 334 and 473 nm with one weak contribution at 587 nm (Figure S26), suggesting that at least one d⁵-oxo unit is required to give rise to the characteristic blue color commonly obtained for iridium precursors oxidized in water, but dimeric Ir^{IV}-O-Ir^{IV} units are more consistent with the high intensities observed experimentally (Figure 15).

As the monomers have their unpaired electrons located in Ir=O d _{π} -p _{π} * orbitals, the formation of the planar Ir^{IV}-O/O-Ir^{IV} core is not due to diradical coupling, but rather results from double donor-acceptor interactions of oxo lone pairs with empty Ir^{IV} d-orbitals. This bonding situation leaves the unpaired electrons on each metal center in the dimer, but with coupling through the delocalized Ir-O/O-Ir π system. Calculation of the triplet state of complex **I** showed that it is

only ~ 0.5 kcal/mol higher in energy, so that an overall singlet ground state with facile S-T interconversion is plausible. As is often seen with such small energy differences, the calculated singlet-triplet gap was found to be highly basis set dependent, however (Table S1).

To further affirm the presence of a bis- μ -oxo structure, we analyzed the blue species of oxidized **3** by Raman spectroscopy. The bis- μ -oxo dimetal unit is a common motif in the active sites of oxidative metalloenzymes,^{103–105} and through detailed analyses of synthetic bis- μ -oxo dimers of Mn,¹⁰⁶ Fe,¹⁰⁷ Co,¹⁰⁸ Ni,¹⁰⁹ and Cu,¹¹⁰ it has been shown that planar M-O/O-M cores exhibit characteristic Raman-active stretches at ~ 550 – 750 cm^{-1} , providing a convenient distinction from other metal-oxo functionalities such as mono- μ -oxo (<500 cm^{-1}), terminal oxo (>900 cm^{-1}), or peroxy units (750 – 850 cm^{-1}).^{111,112}

Raman spectra of solutions of oxidized **3** showed the presence of iodate at its expected position¹¹³ of 800 cm^{-1} irrespective of the excitation wavelength used. Resonance enhancement was observed with either 488 or 660 nm laser excitation to give different sets of molecular signals in the 400 – 900 cm^{-1} fingerprint region characteristic for oxo compounds.¹¹⁴ Except iodate, all peaks observed with 488 nm excitation were found to be insensitive to ¹⁶/¹⁸O substitution (Figure 16, left), consistent with this wavelength being in a regime of pyalc-based electronic transitions that yield resonance-enhancement of ligand-based vibrational modes. This observation is also further experimental support for retention of unmodified (i.e., nonoxygenated) chelate ligand in the blue Cp*Ir^{III}(chelate) precursor.

Excitation in the lower-energy tail of the Ir^{IV}-oxo transitions at 660 nm (cf., Figure 15) yielded different resonance enhancement to give Raman peaks that were not visible with 488 nm excitation (Figure 16, right). Three major new features were located at 559, 610, and 666 cm^{-1} , right in the regime expected for a bis- μ -oxo dimetal unit. Consistently, upon assembly in ¹⁸OH₂ these peaks showed isotopic shifts of 54, 33, and 20 cm^{-1} , respectively, proving that these modes originated from oxo functionalities. Three common features at 752, 880, and 957 cm^{-1} were observed with both λ_{ex} , but no other peaks shifted with ¹⁸O substitution.

Calculation of the Raman-active normal modes of complex **I** with DFT showed several sets of pyalc ligand-based vibrations

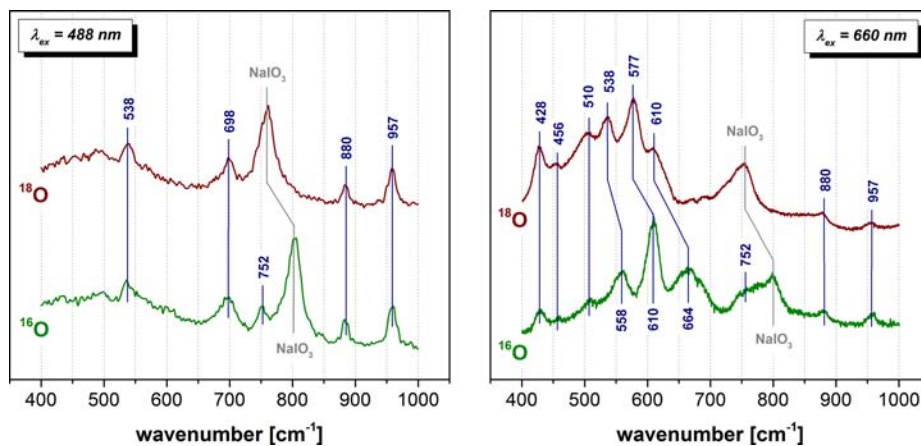
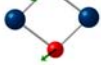
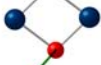
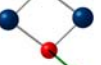



Figure 16. Resonance Raman spectra of solutions **3** (5 mM) oxidized with NaIO₄ (20 mM) in ¹⁶OH₂ (bottom traces) and 95% ¹⁸OH₂ (top traces) after 30 min reaction time as obtained with different excitation energies (left, 488 nm argon-ion laser at 50 mW; right 660 nm diode laser at 17 mW).

Table 2. Characteristic Raman-Active Vibrations of the Planar Bis- μ -oxo Di-iridium(IV) Rhomb of Complex I As Calculated by DFT^a

¹⁶ O (I):	 722 cm ⁻¹	 717 cm ⁻¹	 532 cm ⁻¹	 525 cm ⁻¹
¹⁸ O (I):	687 cm ⁻¹	676 cm ⁻¹	501 cm ⁻¹	497 cm ⁻¹

^aBlue atoms (left/right) = iridium, red atoms (top/bottom) = oxygen; arrows indicate mass-weighted normal mode displacement vectors.

below 1100 cm⁻¹. The peak observed at 957 cm⁻¹ probably corresponds to intense pyridine ring breathing modes involving Ir–N bond stretching calculated at 1055 and 1060 cm⁻¹, and the 880 cm⁻¹ peak likely represents another intense ligand deformation computed at 993 cm⁻¹. Several other sets of medium intensity ligand vibrations were found at 800–750, 700–650, and 470–440 cm⁻¹, but exact assignments of these are difficult due to the strongly coupled nature of these modes. Still, these regimes include or neighbor almost all of the oxygen isotope insensitive peaks experimentally observed with both 488 and 660 nm excitation.

Importantly, none of these coupled modes involved deformation of the bis- μ -oxo core, but two distinct sets of Ir-oxo vibrations were located. One pair of antisymmetric and symmetric Ir–O/O–Ir stretches was found at values of 722 and 717 cm⁻¹, and another pair at 532 and 525 cm⁻¹. As expected, these modes were sensitive to ^{16/18}O substitution with calculated isotopic shifts of 41–28 cm⁻¹ (Table 2).

To demonstrate that Cp* is not needed for homogeneous iridium-catalyzed oxidations, we prepared the corresponding (cod)Ir^I complexes (cod = *cis,cis*-1,5-cyclooctadiene) with the bipy (4) and pyalc (5) ligands as alternative catalyst precursors (Figure 17). Their oxidation should occur very readily, and

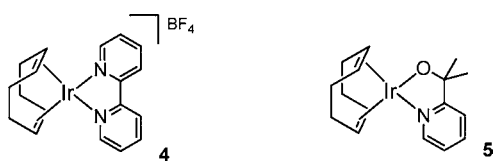


Figure 17. (cod)Ir^I complexes with the bipy (4) and the pyalc (5) ligand.

although some high-valent cod complexes of iridium are known,¹¹⁵ it is rather unlikely that the L₂ hydrocarbon ligand cod remains bound to the iridium under conditions where the more strongly donating L₂X ligand Cp* is lost.

Oxidation of the (cod)Ir^I complexes 4 and 5 with NaIO₄ in H₂O indeed yielded solutions with UV–vis spectra very similar to the ones obtained from the corresponding Cp*Ir^{III} precursors 1 and 3, respectively (Figure 18). Although the kinetics appeared slightly different (Figures S27 and S28), the final λ_{max} values were identical for a given chelate ligand, indicating that the same [Ir^{IV}(chelate)(aqua)_x(oxo)_y]_zⁿ⁺ species had assembled under oxidative conditions irrespective of the sacrificial hydrocarbon ligand in the precursor. Furthermore, the blue species from 4 eventually decayed to a yellow species in solution as it was the case when using 1, whereas the blue species formed from 5 persisted as in the case of 3.

O₂ assays showed that both (cod)Ir^I complexes 4 and 5 were active in O₂ production with aqueous NaIO₄ (Figure 19). Under the conditions applied, all precursors showed an initial lag phase of ~10 s, after which the rate of O₂ evolution quickly reached steady rates. In case of the pyalc precursors, the Cp* complex 3 afforded higher rates than the corresponding cod complex 5, whereas for the bipy ligand the cod complex 4 outperformed the Cp* complex 1. We suspect that the different degradation products of Cp* and cod interfere with WO catalysis, as suggested by the different UV–vis kinetics during oxidation, thereby obscuring clear comparison of performance. NMR analysis of solutions of 4 and 5 oxidized with excess NaIO₄ showed no more signals of the precursors but the presence of small amounts of succinic acid and a hydrophobic precipitate that appeared to be the bis-epoxide of cyclooctadiene.⁶⁰

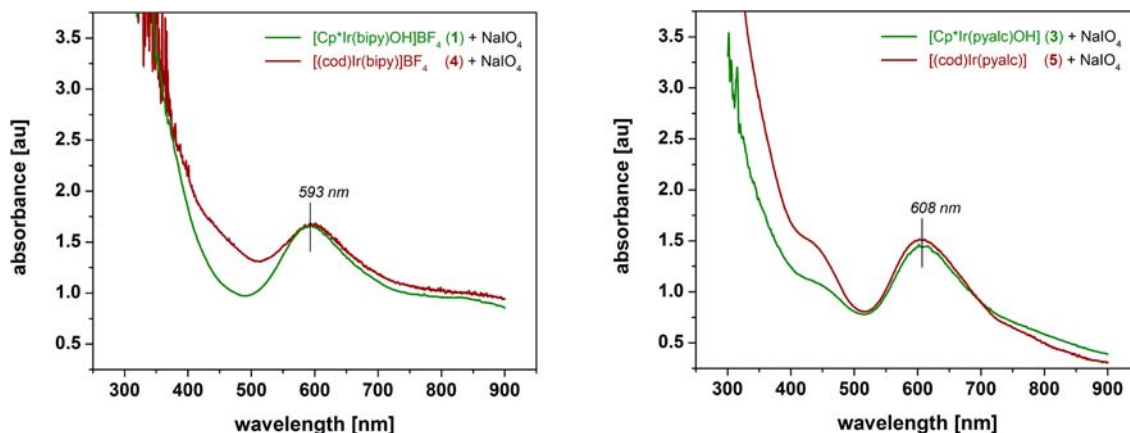


Figure 18. UV–vis spectra of different Ir precursors (1 mM) 30 min after oxidation with NaIO₄ (100 mM) in water.

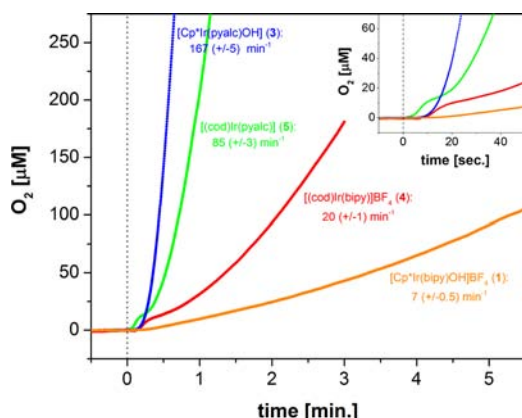


Figure 19. Activities of different Ir precursors (5 μM) in catalytic O_2 evolution with aqueous NaIO_4 (10 mM) at 25 $^\circ\text{C}$ as measured by Clark-type electrode in the liquid phase (rates were determined from the linear regime after initial induction and verified in triplicates). The humps observed shortly after injection of 4 and 5 stem from a small amount of acetone needed to predissolve the cod complexes.

The CH-oxidation ability of the (cod)Ir^I precursors 4 and 5 was also assessed and compared to their Cp*Ir^{III} counterparts 1 and 3. In the aqueous EBS oxidation with NaIO_4 (Scheme 5), all complexes were found to be active (Table 3), and the observed pattern paralleled the respective O_2 evolution performances.

Table 3. Activities of Different Ir Precursors in Catalytic CH-Oxidation with Aqueous NaIO_4 Using 2 μmol of [Ir], 0.2 mmol of EBS, and 2 mmol of NaIO_4 ^a

entry	precatalyst	TOF (5 min) (min^{-1})	TON (30 min)
1	[Cp*Ir(bipy)OH]BF ₄ (1)	0.6 (± 0.5)	7 (± 2)
2	[(cod)Ir(bipy)]BF ₄ (4)	1.2 (± 0.5)	12 (± 2)
3	[Cp*Ir(pyalc)OH] (3)	10.8 (± 0.5)	65 (± 2)
4	[(cod)Ir(pyalc)] (5)	10.2 (± 0.5)	81 (± 2)

^aSee Scheme 5 and Table 1.

These results demonstrate that Cp* is not needed for oxidation catalysis, and that other sacrificial placeholder ligands may be used alternatively as long as one oxidation-resistant chelate ligand is employed. Regardless of the fate of the placeholder ligand in the precursor, however, we believe our originally proposed Ir^{III} \rightarrow Ir^{IV} \rightarrow Ir^V \rightarrow Ir^{III} oxidation cycle² is still the most plausible mechanistic scenario. With a stable LX-type chelate ligand, the blue (IV)–(IV) dimer appears to be the catalyst resting state, which may readily turn over water and hydrocarbon substrates again upon further oxidation. The nuclearity and structural identity of the active Ir^V-oxo species, however, is thus far unknown. Previously, monomeric [Ir(chelate)(H₂O)₂(COOH)Cl] species have been suggested as the activated form of the corresponding [Cp*Ir(chelate)Cl] precursors based on MS analysis,⁴⁴ but in our case we have seen strong evidence for [Ir(chelate)(H₂O)₂(μ -O)]₂ complexes in solution. At least at the millimolar concentrations required for the spectroscopic studies, the dimeric species appear to dominate the solution speciation. Although μ -oxo dimers of high-valent transition metals are known to be rather stable, especially under oxidative conditions at pH values above their pK_a, and in the related ruthenium chemistry the mono- μ -oxo diruthenium unit is retained throughout the water-oxidation

cycle,¹¹⁶ we cannot yet extrapolate whether the same holds true for the iridium system under catalytic conditions (i.e., at micromolar concentrations). As several reports suggest that the Cp*Ir^{III} precursors still provide catalytic activity when immobilized on surfaces via the chelate ligand (site-isolation conditions),^{44,117–119} we believe that monomeric pathways might be accessible too, and we are currently exploring both possibilities in silico. Importantly, the role of the chelate ligand in this chemistry appears to be at least 3-fold: (a) its electronics determine the rate of activation of the precursor as well as (b) the turnover rate in the active form, and (c) its oxidative stability prevents the system from polymerizing to IrO_x. The latter effectively allows water- and CH-oxidations to be run at higher catalyst loadings and milder pH values, two strongly beneficial effects for these difficult reactions. Although our conclusions only strictly apply to the conditions used in this study, and the influence of solvent, pH, concentration, oxidant, etc., on catalyst speciation is well documented in the literature,³⁰ we believe our findings have some general implications for oxidative iridium chemistry.

It is interesting to note that a similar iridium speciation is likely to exist at least initially when precursors lacking oxidation-resistant chelate ligands are employed (e.g., [Cp*Ir-(H₂O)₃]SO₄/[Cp*₂Ir₂(OH)₃]OH or Cp*Ir(L)X₂ complexes), only that these systems ultimately polymerize to heterogeneous iridium-oxide under certain conditions. Particularly, purple-blue [(H₂O)₄Ir^{IV}(μ -OH)₂Ir^{IV}(OH)₂]⁴⁺ dimers have been characterized in dilute aqueous solution of oxidized IrCl₃ with concentrated HClO₄,⁸¹ while at higher pH values and higher iridium concentrations the same reaction serves as a routine procedure for the production of IrO₂ nanoparticles.^{35,36,120–123} It appears plausible that at least some of the reactivity described for IrO_x nanoparticles obtained via this procedure actually stems from the purple-blue aqua-Ir^{IV} dimers present in these mixtures.

A reason for the high activity and remarkable longevity of Ir-based WOCs could be that iridium offers a limited number of stable oxidation states in the range of potentials necessary for catalytic water- and CH-oxidation. Because of the inherent inertness of Ir^{III} and the surprisingly high stability of the Ir^{IV} species demonstrated here, both low-valent states are substitutionally stable, whereas the active Ir^V is electronically inert toward disproportionation into higher oxidation states under WO conditions.¹²⁴ Both channels are known catalyst degradation pathways in water-oxidation mediated by bis- μ -oxo dimanganese complexes.^{125–128} The related mono- μ -oxo diruthenium WOCs do operate in a stable (III)–(IV)–(V)–(III) cycle, but the most highly oxidized form is not electrophilic enough to undergo nucleophilic attack by water, and radical oxo-coupling of two Ru^V-oxo units is typically the RDS in these systems.^{102,116,129,130}

CONCLUSION

Organometallic Cp*Ir^{III} complexes have been shown to rapidly lose their Cp* ligand under oxidative conditions, and water- and CH-oxidation catalysis using these precursors likely proceeds without any bound Cp*. Other sacrificial hydrocarbon ligands like cyclooctadiene can be used alternatively. Placeholder ligands are important because they allow isolation of stable precatalysts while easily generating the reactive species otherwise not accessible. In this vein, the Cp* half-sandwich precursors are still highly practical starting materials because they provide air- and water-stable precursors through versatile

and high-yielding syntheses, but the possibility of using alternative placeholder ligands such as cod will complement the range of accessible precatalysts for both water- and CH-oxidation catalysis. The retained chelate ligand is clearly the most important parameter for tuning the robustness and rate of catalytic water-oxidation, selectivity in CH-oxidation catalysis, and for attachment to surfaces and other aspects of incorporation of these highly active catalysts into electrochemical devices and light-harvesting arrays for solar fuel production.

EXPERIMENTAL SECTION

General. Organic solvents were purified by passing over activated alumina with dry N₂. 18 MΩ cm water was supplied by a Millipore purification system. All chemicals were purchased from major commercial suppliers and used as received. Syntheses were performed under an inert atmosphere of dry N₂ using standard Schlenk techniques. [(η⁵-pentamethylcyclopentadienyl)Ir^{III}(H₂O)₃]SO₄, [(η⁵-pentamethylcyclopentadienyl)Ir^{III}(2,2'-bipyridine-κN,κN')OH]BF₄ (1), and [(η⁵-pentamethylcyclopentadienyl)Ir^{III}(2-(2'-pyridyl)-2-propanolate-κO,κN)OH] (3) were prepared as described previously.^{2,34}

Syntheses. [(η⁵-Pentamethylcyclopentadienyl)Ir^{III}(1,3,5-triazacyclononane-κN,κN,κN)]SO₄ (2). This known compound¹³¹ was prepared via an alternative route. Solid 1,3,5-triazacyclononane (16 mg, 0.12 mmol) was added to an aqueous solution of freshly prepared [Cp*Ir(H₂O)₃]SO₄ (0.1 mmol in 5 mL). The yellow solution was stirred for 16 h at room temperature and then taken to dryness under reduced pressure. The solid residue was taken up in 2 mL of dry methanol, and the solution was filtered through 0.2 μm pore size Teflon filter. Addition of 12 mL of Et₂O caused precipitation of a fine solid, and after removal of the pale yellow supernatant a colorless powder remained, which was dried in vacuo. Yield: 43 mg (78%). ¹H NMR (400 MHz, D₂O): δ = 3.09 (m, 6H), 2.95 (m, 6H), 1.81 (s, 15H). ¹³C NMR (126 MHz, D₂O): δ = 88.1, 52.2, 7.8.

[(η²-*cis,cis*-1,5-Cyclooctadiene)Ir^I(2,2'-bipyridine-κN,κN')]BF₄ (4). This known compound¹³² was prepared via an alternative route. [(cod)IrCl]₂ (67 mg, 0.1 mmol) and 2,2'-bipyridine (31 mg, 0.2 mmol) were combined in dry CH₂Cl₂ (5 mL), immediately yielding a dark purple solution. NaBF₄ (33 mg, 0.3 mmol) in H₂O (3 mL) was added, and the biphasic mixture was stirred vigorously for 1 h at room temperature. The colorless aqueous phase was removed, and the dark brown organic phase was washed with water (2 × 2 mL), and dried over MgSO₄. After filtration through 0.2 μm pore size Teflon filter, Et₂O was added (10 mL), causing precipitation of a fine, dark orange solid, which was collected and dried in vacuo. Yield = 76 mg (70%). ¹H NMR (400 MHz, CD₂Cl₂): δ = 8.46 (d, J = 8.1 Hz, 2H), 8.33 (t, J = 7.7 Hz, 2H), 8.13 (d, J = 5.3 Hz, 2H), 7.75 (t, J = 6.4 Hz, 2H), 4.41 (m, 4H), 2.44 (m, 4H), 2.05 (q, J = 7.9 Hz, 4H). ¹³C NMR (126 MHz, CD₂Cl₂): δ = 158.6, 149.4, 142.9, 128.9, 124.7, 71.2, 31.8.

[(η²-*cis,cis*-1,5-Cyclooctadiene)Ir^I(2-(2'-pyridyl)-2-propanolate-κO,κN)] (5). 2-(2'-Pyridyl)-2-propanol (28 mg, 0.2 mmol) was dissolved in dry THF (10 mL), and ⁿbutyllithium in hexanes (125 μL of a 1.6 M solution, 0.2 mmol) was added dropwise at room temperature. The clear, colorless solution was then added to a solution of [(cod)IrCl]₂ (67 mg, 0.1 mmol) in dry THF (10 mL) via cannula, causing a gradual color change from orange to yellow. The solution was stirred for 10 min at room temperature and then taken to dryness under reduced pressure. Et₂O was added (10 mL) to the solid residue, and the mixture was briefly sonicated, and filtered through 0.2 μm pore size Teflon filter. Evaporation of solvent under reduced pressure and drying in vacuo yielded a yellow-orange powder. Yield = 74 mg (85%). ¹H NMR (400 MHz, CD₂Cl₂): δ = 7.92 (d, J = 5.6 Hz, 1H), 7.80 (td, J = 7.9 Hz, J = 1.5 Hz, 1H), 7.43 (d, J = 8.1 Hz, 1H), 7.20 (ddd, J = 7.2 Hz, J = 5.7 Hz, J = 1.3 Hz, 1H), 4.15 (m, 2H), 3.11 (m, 2H), 2.24 (m, 4H), 1.68 (m, 4H), 1.48 (s, 6H). ¹³C NMR (126 MHz, CD₂Cl₂): δ = 183.0, 146.9, 138.3, 123.1, 122.6, 86.9, 68.1, 52.8, 34.7, 32.7, 31.8. ESI(+)-MS calcd for C₁₆H₂₁IrNO⁺: 434.123, 436.126. Found: m/z = 434.122, 436.125.

Analyses. ¹H and ¹³C NMR spectra were recorded at room temperature on either 400 or 500 MHz Bruker Avance spectrometers and referenced to residual protio-solvent signals (δ in ppm). ¹⁷O NMR was performed on a 500 MHz Bruker Avance spectrometer equipped with a 5 mm ATMA broadband probe operating at 67.8 MHz controlled through TopSpin (version 1.3). Samples were prepared by dissolving the solid reagents in 10% ¹⁷OH₂ (Enrichment Technologies LTD) at least 15 min prior to the analysis. Measurements were performed with sample spinning but without lock and sweep using the following parameters: p1 = 10 μs, d1 = 100 ms, aq = 100 ms, sw = 1400 ppm, ns = 150,000. Spectra were manually phased and baseline corrected with apodization to 20 Hz line broadening, and the free water line centered to 0 ppm. Paramagnetic susceptibility measurements by ¹H NMR were performed at room temperature on a 400 MHz Bruker Avance spectrometer. A 10 mM solution of 3 was oxidized with 200 mM NaIO₄ for 30 min in D₂O, and 0.4 mL of the resulting blue solution was transferred to a 5 mm NMR sample tube. A coaxial insert containing 200 mM NaIO₃ in D₂O was added, and ¹H NMR spectra were acquired with and without the reference solution. The shift difference of the H₂O signal was converted to χ_m using the Evans method with Schubert's correction for superconducting magnets,¹³³ and μ_{eff} calculated using the Curie law with spin-only approximation.¹³⁴

UV-vis spectra were recorded at 1 nm resolution on a Varian Cary 50 using 1.0 cm quartz cuvettes against a background of neat solvent. Kinetics were monitored with 0.2 Hz at the wavelength stated.

MALDI-TOF-MS measurements were performed using an Applied Biosystems (AB)/MDS Sciex model 4800 MALDI-TOF/TOF mass spectrometer with AB 4000 Series Explorer software (version 3.6). An aqueous solution of 0.1 mM 3 and 1 mM NaIO₄ was stirred for ~2 min at room temperature, after which a 1 μL aliquot was withdrawn and mixed with 99 μL of matrix solution (16 mM α-cyano-4-hydroxycinnamic acid in 1:1 MeCN/H₂O). One microliter portions of the quenched mixture were spotted onto the MALDI target plate, dried in air, introduced to the HV chamber, and ionized with a YAG laser at 355 nm (200 Hz). Spectra were acquired over the mass range 300–2000 m/z in reflector positive mode summing 2000 laser shots.

Planar electrophoresis was performed on a BioRad EPS 301 setup using glass microfiber pads (Whatman) as stationary phase wetted with 100 mM NaIO₃ electrolyte solution.

TEM images and EDX spectra were taken using a FEI Osiris 200 kV TEM. Samples were prepared by oxidizing a 5 mM aqueous solution of 3 with 200 mM NaIO₄ for 1 h at room temperature, evaporation of solvent at 50 °C, drying in high vacuum, and depositing the resulting bluish powder onto SiO or lacey carbon copper TEM grids (Ted Pella) as a suspension in dry CH₂Cl₂. Peak deconvolutions were performed using TIA software.

XPS spectroscopy was performed using aluminum Kα photons (hν = 1486.6 eV) and a double-pass cylinder mirror analyzer (PHI 15-255G). Samples were prepared by pressing some of the solid sample prepared for TEM-EDX onto a 0.1 mm thick disc (1 cm diameter) of high-purity gold (99.99%, Ted Pella) using a benchtop pellet press at 2000 psi. Spectra were referenced using gold as internal standard, and peak fits were performed using XPSPeak (version 4.1).

EPR spectroscopy was performed on a 9.2 GHz X-band Bruker ELEXSYS E500 spectrometer equipped with an Oxford ESR-900 cryostat at 7 K. A 100 μM solution of 3 was oxidized with 10 mM NaIO₄ for 10 min, frozen with liquid nitrogen, and placed in the spectrometer for analysis.

Raman spectra were collected on a Spex 1403 Ramalog Double Laser-Raman spectrometer interfaced with a Spex DM3000 data acquisition system (used in direct photon-counting mode) and based upon a Spectra-Physics Stablite 2017 argon-ion laser or a Horiba Jobin-Yvon T64000 Raman spectrometer with triple subtractive monochromator and an Ignis 660 diode laser. Samples were prepared in spectral grade water at least 30 min prior to the analysis, and a background of pure water was collected before the sample was measured at room temperature (5 s integration time at 2 cm⁻¹ resolution [Spex] or 60 s integration time at 0.1 cm⁻¹ resolution [Horiba]). Raman-shift calibrations were performed by either scanning

over the excitation line (Spex, with reduced slit width) or with a silicon reference sample (Horiba). Plasma lines from the argon-ion excitation source were manually removed from the 488 nm spectrum, which then was interpolated with a B-spline function.

O₂ assays were run at 25 °C using a temperature-controlled YSI Clark-type electrode setup. After zeroing with NaHSO₃ solution, the electrode was allowed to stabilize in 5 mL of a freshly prepared, air-saturated aqueous oxidant solution (10 mM NaIO₄) for 3–5 min with stirring before injecting 250 μL of a 0.1 mM catalyst solution to start the catalysis. Averages of 100,000 individual data points were collected with 6 Hz until saturation of the electrode (~250 μM O₂).

CH-oxidations were run by predissolving 0.2 mmol of substrate (42 mg of EBS) and 2 mmol of oxidant (428 mg of NaIO₄) in 5 mL of water at room temperature, and then injecting 200 μL of a 10 mM catalyst solution to start the reaction. Conversions were determined from ¹H NMR using 40 mM sodium *d*₄-trimethylsilylpropionate as internal standard.

■ ASSOCIATED CONTENT

● Supporting Information

Additional ¹H and ¹⁷O NMR spectra, UV–vis spectra, O₂ assays, MALDI-TOF-MS spectra, (HR)TEM images, EDX and XPS spectra, xyz coordinates, and full reference 99. This material is available free of charge via the Internet at <http://pubs.acs.org>.

■ AUTHOR INFORMATION

Corresponding Author

dhe@chem.byu.edu; richens@nmsu.edu; patrick.vaccaro@yale.edu; gary.brudvig@yale.edu; robert.crabtree@yale.edu

Present Addresses

^{||}Centre for Sustainable Chemical Technologies, University of Bath, Bath BA2 7AY, United Kingdom.

[⊥]International Institute for Carbon-Neutral Energy Research (WPI-I²CNER), Kyushu University, Motooka 744, Nishi-ku, Fukuoka 819-0395, Japan.

Notes

The authors declare no competing financial interest.

■ ACKNOWLEDGMENTS

This material is based in part upon work supported by the Center for Catalytic Hydrocarbon Functionalization, an Energy Frontier Research Center funded by the U.S. Department of Energy, Office of Science, Office of Basic Energy Sciences, under Award Number DE-SC0001298 (U.H. and R.H.C., CH-oxidation; D.H.E., theory), and by the NSF GRFP and the Division of Chemical Sciences, Geosciences, and Biosciences, Office of Basic Energy Sciences of the U.S. Department of Energy (DE-FG02-07ER15909) (S.W.S., A.R.P., and G.W.B., water-oxidation). Facilities used were supported by the Yale Institute for Nanoscience and Quantum Engineering (YINQE), the Yale Center for Research on Interface Structures and Phenomena (CRISP), and NSF MRSEC DMR 1119826. U.H. thanks the Alexander von Humboldt Foundation for a Feodor Lynen Research Fellowship, supplemented by a grant from the YINQE. S.W.S. and A.R.P. were supported by NSF Graduate Research Fellowships. P.H.V. acknowledges continuing support of the U.S. National Science Foundation under the auspices of Grant CHE-1112239 (Raman spectroscopy). D.T.R. thanks New Mexico State University. We thank Jean Kanyo, Kathryn Stone, Edward Voss, and TuKiet Lam (Mass Spectrometry and Proteomics Resource of the W.M. Keck Foundation Biotechnology Resource Laboratory at Yale University) for MS analyses, and Eric Paulson (CBIC Yale) for help with ¹⁷O NMR

measurements. Charles Ahn, Fred Walker, and Lior Kornblum (CRISP Yale) are acknowledged for access to XPS, Michael Rooks and the YINQE for TEM/SEM/EDX, and Mark Schwab (C&EE Yale) for Raman spectroscopy. We thank Nathan Schley (Caltech), Meng Zhou (Rutgers University), and Marc Zimmer (Connecticut College) for valuable discussions.

■ REFERENCES

- (1) Hull, J. F.; Balcells, D.; Blakemore, J. D.; Incarvito, C. D.; Eisenstein, O.; Brudvig, G. W.; Crabtree, R. H. *J. Am. Chem. Soc.* **2009**, *131*, 8730.
- (2) Blakemore, J. D.; Schley, N. D.; Balcells, D.; Hull, J. F.; Olack, G. W.; Incarvito, C. D.; Eisenstein, O.; Brudvig, G. W.; Crabtree, R. H. *J. Am. Chem. Soc.* **2010**, *132*, 16017.
- (3) Lalrempuia, R.; McDaniel, N. D.; Müller-Bunz, H.; Bernhard, S.; Albrecht, M. *Angew. Chem., Int. Ed.* **2010**, *49*, 9765.
- (4) Savini, A.; Bellachioma, G.; Ciancaleoni, G.; Zuccaccia, C.; Zuccaccia, D.; Macchioni, A. *Chem. Commun.* **2010**, *46*, 9218.
- (5) Hettterscheid, D. G. H.; Reek, J. N. H. *Chem. Commun.* **2011**, *47*, 2712.
- (6) Grotjahn, D. B.; Brown, D. B.; Martin, J. K.; Marelus, D. C.; Abadjian, M.-C.; Tran, H. N.; Kalyuzhny, G.; Vecchio, K. S.; Specht, Z. G.; Cortes-Llamas, S. A.; Miranda-Soto, V.; van Niekerk, C.; Moore, C. E.; Rheingold, A. L. *J. Am. Chem. Soc.* **2011**, *133*, 19024.
- (7) Hong, D.; Murakami, M.; Yamada, Y.; Fukuzumi, S. *Energy Environ. Sci.* **2012**, *5*, 5708.
- (8) Bucci, A.; Savini, A.; Rocchigiani, L.; Zuccaccia, C.; Rizzato, S.; Albinati, A.; Llobet, A.; Macchioni, A. *Organometallics* **2012**, *31*, 8071.
- (9) Codolà, Z.; Cardoso, M. S. J.; Royo, B.; Costas, M.; Lloret-Fillol, J. *Chem.-Eur. J.* **2013**, *19*, 7203.
- (10) Zhou, M.; Schley, N. D.; Crabtree, R. H. *J. Am. Chem. Soc.* **2010**, *132*, 12550.
- (11) Zhou, M.; Balcells, D.; Parent, A. R.; Crabtree, R. H.; Eisenstein, O. *ACS Catal.* **2012**, *2*, 208.
- (12) Zhou, M.; Hintermair, U.; Hashiguchi, B. G.; Parent, A. R.; Hashmi, S. M.; Elimelech, M.; Periana, R. A.; Brudvig, G. W.; Crabtree, R. H. *Organometallics* **2013**, *32*, 957.
- (13) Bockris, J. O. M. *Energy: The Solar-Hydrogen Alternative*, 1st ed.; Halsted Press: New York, 1975.
- (14) Grätzel, M. *Acc. Chem. Res.* **1981**, *14*, 376.
- (15) Meyer, T. J. *Acc. Chem. Res.* **1989**, *22*, 163.
- (16) Lewis, N. S.; Nocera, D. G. *Proc. Natl. Acad. Sci. U.S.A.* **2006**, *103*, 15729.
- (17) Gust, D.; Moore, T. A.; Moore, A. L. *Acc. Chem. Res.* **2009**, *42*, 1890.
- (18) Walter, M. G.; Warren, E. L.; McKone, J. R.; Boettcher, S. W.; Mi, Q.; Santori, E. A.; Lewis, N. S. *Chem. Rev.* **2010**, *110*, 6446.
- (19) Crabtree, R. H. *Energy Production and Storage - Inorganic Chemistry Strategies for a Warming World*; John Wiley & Sons: Hoboken, 2010.
- (20) Young, K. J.; Martini, L. A.; Milot, R. L.; Snoeberger, R. C.; Batista, V. S.; Schmuttenmaer, C. A.; Crabtree, R. H.; Brudvig, G. W. *Coord. Chem. Rev.* **2012**, *256*, 2503.
- (21) Dau, H.; Limberg, C.; Reier, T.; Risch, M.; Roggan, S.; Strasser, P. *ChemCatChem* **2010**, *2*, 724.
- (22) Shilov, A. E.; Shteinman, A. A. *Coord. Chem. Rev.* **1977**, *24*, 97.
- (23) Crabtree, R. H. *Chem. Rev.* **1985**, *85*, 245.
- (24) Labinger, J. A.; Bercaw, J. E. *Nature* **2002**, *417*, 507.
- (25) Gunay, A.; Theopold, K. H. *Chem. Rev.* **2010**, *110*, 1060.
- (26) Chen, M. S.; White, M. C. *Science* **2007**, *318*, 783.
- (27) Que, L.; Tolman, W. B. *Nature* **2008**, *455*, 333.
- (28) Zhou, M.; Crabtree, R. H. *Chem. Soc. Rev.* **2011**, *40*, 1875.
- (29) Hashiguchi, B. G.; Bischof, S. M.; Konnick, M. M.; Periana, R. A. *Acc. Chem. Res.* **2012**, *45*, 885.
- (30) Artero, V.; Fontecave, M. *Chem. Soc. Rev.* **2013**, *42*, 2338.
- (31) Wasylenko, D. J.; Palmer, R. D.; Berlinguette, C. P. *Chem. Commun.* **2013**, *49*, 218.

- (32) Brewster, T. P.; Blakemore, J. D.; Schley, N. D.; Incarvito, C. D.; Hazari, N.; Brudvig, G. W.; Crabtree, R. H. *Organometallics* **2011**, *30*, 965.
- (33) Graeupner, J.; Brewster, T. P.; Blakemore, J. D.; Schley, N. D.; Thomsen, J. M.; Brudvig, G. W.; Hazari, N.; Crabtree, R. H. *Organometallics* **2012**, *31*, 7158.
- (34) Hintermair, U.; Hashmi, S. M.; Elimelech, M.; Crabtree, R. H. *J. Am. Chem. Soc.* **2012**, *134*, 9785.
- (35) Wöhler, L.; Witzmann, W. Z. *Anorg. Chem.* **1908**, *57*, 323.
- (36) Harriman, A.; Thomas, J. M.; Millward, G. R. *New J. Chem.* **1987**, *11*, 757.
- (37) Schley, N. D.; Blakemore, J. D.; Subbaiyan, N. K.; Incarvito, C. D.; D'Souza, F.; Crabtree, R. H.; Brudvig, G. W. *J. Am. Chem. Soc.* **2011**, *133*, 10473.
- (38) Miguel-Garcia, J. A.; Maitlis, P. M. *J. Chem. Soc., Chem. Commun.* **1990**, 1472.
- (39) Fan, L.; Turner, M. L.; Hursthouse, M. B.; Malik, K. M. A.; Gusev, O. V.; Maitlis, P. M. *J. Am. Chem. Soc.* **1994**, *116*, 385.
- (40) Fujita, K.-i.; Nakamura, M.; Yamaguchi, R. *Organometallics* **2000**, *20*, 100.
- (41) Park-Gehrke, L. S.; Freudenthal, J.; Kaminsky, W.; DiPasquale, A. G.; Mayer, J. M. *Dalton Trans.* **2009**, 1972.
- (42) Savini, A.; Belanzoni, P.; Bellachioma, G.; Zuccaccia, C.; Zuccaccia, D.; Macchioni, A. *Green Chem.* **2011**, *13*, 3360.
- (43) Zuccaccia, C.; Bellachioma, G.; Bolaño, S.; Rocchigiani, L.; Savini, A.; Macchioni, A. *Eur. J. Inorg. Chem.* **2012**, 1462.
- (44) Wang, C.; Wang, J.; Lin, W. *J. Am. Chem. Soc.* **2012**, *134*, 19895.
- (45) Parent, A. R.; Brewster, T. P.; De Wolf, W.; Crabtree, R. H.; Brudvig, G. W. *Inorg. Chem.* **2012**, *51*, 6147.
- (46) Parent, A. R.; Crabtree, R. H.; Brudvig, G. W. *Chem. Soc. Rev.* **2013**, *42*, 2247.
- (47) Crabtree, R. H. *Chem. Rev.* **2012**, *112*, 1536.
- (48) Petronilho, A.; Rahman, M.; Woods, J. A.; Al-Sayyed, H.; Müller-Bunz, H.; Don MacElroy, J. M.; Bernhard, S.; Albrecht, M. *Dalton Trans.* **2012**, *41*, 13074.
- (49) Heaton, B. *Mechanisms in Homogeneous Catalysis*; Wiley-VCH: Weinheim, 2005.
- (50) The low concentrations required for this experiment to be monitored by Clark electrode likely cause oxygen production to stall below a certain solution potential, therefore not reaching the theoretical amount of 17 equiv of O₂. At higher concentrations, >90% O₂ evolution efficiency has been reported for other Cp*Ir precatalysts with aqueous NaO₄.⁹
- (51) Herberhold, M.; Kremnitz, W.; Razavi, A.; Schöllhorn, H.; Thewalt, U. *Angew. Chem., Int. Ed. Engl.* **1985**, *24*, 601.
- (52) Trost, M. K.; Bergman, R. G. *Organometallics* **1991**, *10*, 1172.
- (53) Faller, J. W.; Ma, Y. *Organometallics* **1988**, *7*, 559.
- (54) Herrmann, W. A.; Serrano, R.; Bock, H. *Angew. Chem.* **1984**, *96*, 364.
- (55) Rao, K. M.; Day, C. L.; Jacobson, R. A.; Angelici, R. J. *Organometallics* **1992**, *11*, 2303.
- (56) Kirchner, K.; Mauthner, K.; Mereiter, K.; Schmid, R. *J. Chem. Soc., Chem. Commun.* **1993**, *0*, 892.
- (57) Gross, C. L.; Brumaghim, J. L.; Girolami, G. S. *Organometallics* **2007**, *26*, 2258.
- (58) Winkler, J. R.; Gray, H. B. In *Molecular Electronic Structures of Transition Metal Complexes I*; Mingos, D. M. P., Day, P., Dahl, J. P., Eds.; Springer: Berlin Heidelberg: 2012; Vol. 142, p 17.
- (59) Hay-Motherwell, R. S.; Wilkinson, G.; Hussain-Bates, B.; Hursthouse, M. B. *Polyhedron* **1993**, *12*, 2009.
- (60) A more detailed MS study on the oxidative activation of these precursors is currently under way and will be reported elsewhere in due course.
- (61) Castillo-Blum, S. E.; Richens, D. T.; Sykes, A. G. *J. Chem. Soc., Chem. Commun.* **1986**, 1120.
- (62) Dass, A.; Stevenson, A.; Dubay, G. R.; Tracy, J. B.; Murray, R. W. *J. Am. Chem. Soc.* **2008**, *130*, 5940.
- (63) Kim, B. H.; Shin, K.; Kwon, S. G.; Jang, Y.; Lee, H.-S.; Lee, H.; Jun, S. W.; Lee, J.; Han, S. Y.; Yim, Y.-H.; Kim, D.-H.; Hyeon, T. *J. Am. Chem. Soc.* **2013**, *135*, 2407.
- (64) Khitrov, G. A.; Strouse, G. F. *J. Am. Chem. Soc.* **2003**, *125*, 10465.
- (65) Xue, G.; Dai, Q.; Jiang, S. *J. Am. Chem. Soc.* **1988**, *110*, 2393.
- (66) Weldon, M. K.; Uvdal, P.; Friend, C. M.; Serafin, J. G. *J. Chem. Phys.* **1995**, *103*, 5075.
- (67) Kim, Y. L.; Hatfield, W. E. *Inorg. Chim. Acta* **1991**, *188*, 15.
- (68) Uemura, S.; Spencer, A.; Wilkinson, G. *J. Chem. Soc., Dalton Trans.* **1973**, 2565.
- (69) Hills, E. F.; Richens, D. T.; Sykes, A. G. *Inorg. Chem.* **1986**, *25*, 3144.
- (70) Alternatively, the EPR signal could be very broad and thus hard to detect.
- (71) Kölle, U. *Coord. Chem. Rev.* **1994**, *135–136*, 623.
- (72) Richens, D. T. *The Chemistry of Aqua Ions - Synthesis, Structure & Reactivity*, 1st ed.; John Wiley & Sons Ltd.: Chichester, 1997.
- (73) Richens, D. T. *Comm. Inorg. Chem.* **2005**, *26*, 217.
- (74) Jentsch, W.; Schmidt, W.; Sykes, A. G.; Wieghardt, K. *Inorg. Chem.* **1977**, *16*, 1935.
- (75) Wieghardt, K.; Schmidt, W.; Nuber, B.; Weiss, J. *Chem. Ber.* **1979**, *112*, 2220.
- (76) Taylor, R. S.; Sykes, A. G. *Inorg. Chem.* **1974**, *13*, 2524.
- (77) Wieghardt, K.; Schmidt, W.; Nuber, B.; Prikner, B.; Weiss, J. *Chem. Ber.* **1980**, *113*, 36.
- (78) Hancock, M.; Nielsen, B.; Springborg, J. *Acta Chem. Scand.* **1982**, *36A*, 313.
- (79) Christensson, F.; Springborg, J. *Inorg. Chem.* **1985**, *24*, 2129.
- (80) Galsbøl, F.; Larsen, S.; Rasmussen, B.; Springborg, J. *Inorg. Chem.* **1986**, *25*, 290.
- (81) Castillo-Blum, S. E.; Richens, D. T.; Sykes, A. G. *Inorg. Chem.* **1989**, *28*, 954.
- (82) Richens, D. T. *Chem. Rev.* **2005**, *105*, 1961.
- (83) Balogh, E.; Casey, W. H. *Prog. Nucl. Magn. Reson. Spectrosc.* **2008**, *53*, 193.
- (84) Lieb, D.; Zahl, A.; Wilson, E. F.; Streb, C.; Nye, L. C.; Meyer, K.; Ivanović-Burmazović, I. *Inorg. Chem.* **2011**, *50*, 9053.
- (85) Ohlin, C. A.; Harley, S. J.; McAlpin, J. G.; Hocking, R. K.; Mercado, B. Q.; Johnson, R. L.; Villa, E. M.; Fidler, M. K.; Olmstead, M. M.; Spiccia, L.; Britt, R. D.; Casey, W. H. *Chem.-Eur. J.* **2011**, *17*, 4408.
- (86) Cusanelli, A.; Frey, U.; Richens, D. T.; Merbach, A. E. *J. Am. Chem. Soc.* **1996**, *118*, 5265.
- (87) Dacj, L.; Elias, H.; Frey, U.; Hörnig, A.; Kölle, U.; Merbach, A. E.; Paulus, H.; Schneider, J. S. *Inorg. Chem.* **1995**, *34*, 306.
- (88) Poth, T.; Paulus, H.; Elias, H.; Dücker-Benfer, C.; van Eldik, R. *Eur. J. Inorg. Chem.* **2001**, *2001*, 1361.
- (89) Schley, N. D.; Halbert, S.; Raynaud, C.; Eisenstein, O.; Crabtree, R. H. *Inorg. Chem.* **2012**, *51*, 12313.
- (90) Dove, M. F. A.; Sanders, J. C. P.; Appelman, E. H. *Magn. Reson. Chem.* **1995**, *33*, 44.
- (91) Pecht, I.; Luz, Z. *J. Am. Chem. Soc.* **1965**, *87*, 4068.
- (92) Dwek, R. A.; Luz, Z.; Peller, S.; Shporer, M. *J. Am. Chem. Soc.* **1971**, *93*, 77.
- (93) Anbar, M.; Guttmann, S. *J. Am. Chem. Soc.* **1961**, *83*, 781.
- (94) Wharton, R. K.; Taylor, R. S.; Sykes, A. G. *Inorg. Chem.* **1975**, *14*, 33.
- (95) Gamsjäger, H.; Beutler, P. *J. Chem. Soc., Dalton Trans.* **1979**, 1415.
- (96) Christ, H. A.; Diehl, P.; Schneider, H.; Dahn, H. *Helv. Chim. Acta* **1961**, *44*, 865.
- (97) O'Connor, C.; Turney, T. A. *J. Chem. Soc. B* **1966**, 1211.
- (98) Boykin, D. W. *¹⁷O NMR Spectroscopy in Organic Chemistry*, 1st ed.; CRC Press: Boca Raton, FL, 1991.
- (99) Frisch, M. J.; et al. *Gaussian 09*, revision B.01; Gaussian, Inc.: Wallingford, CT, 2009.
- (100) Zhao, Y.; Truhlar, D. G. *Acc. Chem. Res.* **2008**, *41*, 157.

- (101) Tomasi, J.; Mennucci, B.; Cammi, R. *Chem. Rev.* **2005**, *105*, 2999.
- (102) Gersten, S. W.; Samuels, G. J.; Meyer, T. J. *J. Am. Chem. Soc.* **1982**, *104*, 4029.
- (103) Que, L.; Dong, Y. *Acc. Chem. Res.* **1996**, *29*, 190.
- (104) Tolman, W. B. *Acc. Chem. Res.* **1997**, *30*, 227.
- (105) Manchanda, R.; Brudvig, G. W.; Crabtree, R. H. *Coord. Chem. Rev.* **1995**, *144*, 1.
- (106) Cua, A.; Vrettos, J.; Paula, J.; Brudvig, G.; Bocian, D. *J. Biol. Inorg. Chem.* **2003**, *8*, 439.
- (107) Wilkinson, E. C.; Dong, Y.; Zang, Y.; Fujii, H.; Fraczkiewicz, R.; Fraczkiewicz, G.; Czernuszewicz, R. S.; Que, L. *J. Am. Chem. Soc.* **1998**, *120*, 955.
- (108) Hikichi, S.; Yoshizawa, M.; Sasakura, Y.; Akita, M.; Moro-oka, Y. *J. Am. Chem. Soc.* **1998**, *120*, 10567.
- (109) Itoh, S.; Bandoh, H.; Nakagawa, M.; Nagatomo, S.; Kitagawa, T.; Karlin, K. D.; Fukuzumi, S. *J. Am. Chem. Soc.* **2001**, *123*, 11168.
- (110) Holland, P. L.; Cramer, C. J.; Wilkinson, E. C.; Mahapatra, S.; Rodgers, K. R.; Itoh, S.; Taki, M.; Fukuzumi, S.; Que, L.; Tolman, W. B. *J. Am. Chem. Soc.* **2000**, *122*, 792.
- (111) Solomon, E. I.; Tuzcek, F.; Root, D. E.; Brown, C. A. *Chem. Rev.* **1994**, *94*, 827.
- (112) Henson, M. J.; Mukherjee, P.; Root, D. E.; Stack, T. D. P.; Solomon, E. I. *J. Am. Chem. Soc.* **1999**, *121*, 10332.
- (113) Gardiner, D. J.; Girling, R. B.; Hester, R. E. *J. Mol. Struct.* **1972**, *13*, 105.
- (114) Nakamoto, K. *Infrared and Raman Spectra of Inorganic and Coordination Compounds*, 6th ed.; John Wiley & Sons, Ltd.: Hoboken, 2009.
- (115) Lange, C. W.; Pierpont, C. G. *J. Am. Chem. Soc.* **1992**, *114*, 6582.
- (116) Gilbert, J. A.; Eggleston, D. S.; Murphy, W. R.; Geselowitz, D. A.; Gersten, S. W.; Hodgson, D. J.; Meyer, T. J. *J. Am. Chem. Soc.* **1985**, *107*, 3855.
- (117) Moore, G. F.; Blakemore, J. D.; Milot, R. L.; Hull, J. F.; Song, H.-e.; Cai, L.; Schmuttenmaer, C. A.; Crabtree, R. H.; Brudvig, G. W. *Energy Environ. Sci.* **2011**, *4*, 2389.
- (118) Joya, K. S.; Subbaiyan, N. K.; D'Souza, F.; de Groot, H. J. M. *Angew. Chem., Int. Ed.* **2012**, *51*, 9601.
- (119) Vagnini, M. T.; Smeigh, A. L.; Blakemore, J. D.; Eaton, S. W.; Schley, N. D.; D'Souza, F.; Crabtree, R. H.; Brudvig, G. W.; Co, D. T.; Wasielewski, M. R. *Proc. Natl. Acad. Sci. U.S.A.* **2012**, *109*, 15651.
- (120) Gambardella, A. A.; Bjorge, N. S.; Alspaugh, V. K.; Murray, R. W. *J. Phys. Chem. C* **2011**, *115*, 21659.
- (121) Zhao, Y.; Hernandez-Pagan, E. A.; Vargas-Barbosa, N. M.; Dysart, J. L.; Mallouk, T. E. *J. Phys. Chem. Lett.* **2011**, *2*, 402.
- (122) Frame, F. A.; Townsend, T. K.; Chamousis, R. L.; Sabio, E. M.; Dittrich, T.; Browning, N. D.; Osterloh, F. E. *J. Am. Chem. Soc.* **2011**, *133*, 7264.
- (123) Sivasankar, N.; Weare, W. W.; Frei, H. *J. Am. Chem. Soc.* **2011**, *133*, 12976.
- (124) Riedel, S.; Kaupp, M. *Angew. Chem., Int. Ed.* **2006**, *45*, 3708.
- (125) Limburg, J.; Brudvig, G. W.; Crabtree, R. H. *J. Am. Chem. Soc.* **1997**, *119*, 2761.
- (126) Limburg, J.; Vrettos, J. S.; Liable-Sands, L. M.; Rheingold, A. L.; Crabtree, R. H.; Brudvig, G. W. *Science* **1999**, *283*, 1524.
- (127) Limburg, J.; Vrettos, J. S.; Chen, H.; de Paula, J. C.; Crabtree, R. H.; Brudvig, G. W. *J. Am. Chem. Soc.* **2001**, *123*, 423.
- (128) Chen; Tagore, R.; Olack, G.; Vrettos, J. S.; Weng, T.-C.; Penner-Hahn, J.; Crabtree, R. H.; Brudvig, G. W. *Inorg. Chem.* **2007**, *46*, 34.
- (129) Binstead, R. A.; Chronister, C. W.; Ni, J.; Hartshorn, C. M.; Meyer, T. J. *J. Am. Chem. Soc.* **2000**, *122*, 8464.
- (130) Hurst, J. K. *Coord. Chem. Rev.* **2005**, *249*, 313.
- (131) Grant, G. J.; Lee, J. P.; Helm, M. L.; VanDerveer, D. G.; Pennington, W. T.; Harris, J. L.; Mehne, L. F.; Klinger, D. W. *J. Organomet. Chem.* **2005**, *690*, 629.
- (132) Mestroni, G.; Camus, A.; Zassinovich, G. *J. Organomet. Chem.* **1974**, *73*, 119.
- (133) Schubert, E. M. *J. Chem. Educ.* **1992**, *69*, 62.
- (134) De Buysser, K.; Herman, G. G.; Bruneel, E.; Hoste, S.; Van Driessche, I. *Chem. Phys.* **2005**, *315*, 286.